

---

---

# ***Louisiana Transportation Research Center***

---

---

Final Report 608

## **Impact of Inundation on Roadway Pavements: Case Study – LA 493**

by

Kevin Gaspard  
Zhongjie Zhang  
Gavin Gautreau  
Murad Abufarsakh  
Mark Martinez

**LTRC**

---

---



4101 Gourrier Avenue | Baton Rouge, Louisiana 70808  
(225) 767-9131 | (225) 767-9108 fax | [www.ltrc.lsu.edu](http://www.ltrc.lsu.edu)

**TECHNICAL REPORT STANDARD PAGE**

1. Report No. <b>FHWA/LA.18/608</b>		2. Government Accession No.		3. Recipient's Catalog No.	
4. Title and Subtitle <b>Impact of Inundation on Roadway Pavements: Case Study – LA 493</b>		5. Report Date May 2019		6. Performing Organization Code LTRC Project Number: 12-1P SIO Number: 30000607	
		7. Author(s) Kevin Gaspard, Zhongjie Zhang, Gavin Gautreau, Murad Abufarsakh, and Mark Martinez			
9. Performing Organization Name and Address  Department of Civil and Environmental Engineering Louisiana State University Baton Rouge, LA 70803		10. Work Unit No.		11. Contract or Grant No.	
		12. Sponsoring Agency Name and Address Louisiana Department of Transportation and Development P.O. Box 94245 Baton Rouge, LA 70804-9245			
		14. Sponsoring Agency Code			
15. Supplementary Notes <b>Conducted in Cooperation with the U.S. Department of Transportation, Federal Highway Administration</b>					
16. Abstract LTRC has conducted a research study on LA 493 that provides evidence of damage to roadways caused by inundation. The evidence supporting this comes from three sources: a rod and level cross-section survey taken approximately one month prior to the first inundation event and subsequent cross-section surveys taken after the first to third inundation events; from pavement assessments with LTRC's profiler in June 2017 and June 2018; and from a structural assessment with the falling weight deflectometer (FWD).  Differential movements of the roadway surface were measured after the inundation events. The elevation increase at the centerline of the test sites varied from 2.44 mm to 44.5 mm after the first inundation event. Movements such as those measured will adversely affect the pavements performance leading to a reduced service life.  Results from the IRI testing implied that (1) there were high degrees of differential profile changes in the roadway surface, (2) the IRI was significantly higher than it should have been for a roadway with its service age, and (3) there was a high degree of IRI variation amongst the test sites. Data from rutting tests also had high degrees of variability. The maximum measured rut depth was 1.685 in.  Longitudinal crack data implied that (1) most of the sites had excessive longitudinal cracking for the time that they were in service, (2) the longitudinal cracking observed is consistent with volumetric changes occurring in the subgrade, and (3) it is logical to infer that the inundation events were responsible for both the magnitude and premature emergence of these longitudinal cracks.  Data from the FWD testing implied that structural damage was present. The amount of damage present ranged from 0.2 to 2.61 in. of equivalent asphaltic concrete thickness.					
17. Key Words		18. Distribution Statement <b>Unrestricted. This document is available through the National Technical Information Service, Springfield, VA 21161.</b>			
19. Security Classif. (of this report)	20. Security Classif. (of this page)	21. No. of Pages		22. Price	

## **Project Review Committee**

Each research project will have an advisory committee appointed by the LTRC Director. The Project Review Committee is responsible for assisting the LTRC Administrator or Manager in the development of acceptable research problem statements, requests for proposals, review of research proposals, oversight of approved research projects, and implementation of findings.

LTRC appreciates the dedication of the following Project Review Committee Members in guiding this research study to fruition.

### ***LTRC Administrator***

Zhongjie Zhang

Pavement and Geotechnical Research Administrator

### ***Members***

Jonathan Lachney

Matthew Ziecker

Ken Free

Mark Chenevert

Jeff Lambert

Hallie Dozier

Scott Nelson

### ***Directorate Implementation Sponsor***

Christopher P. Knotts, P.E.

DOTD Chief Engineer

# **Impact of Inundation on Roadway Pavements: Case Study – LA 493**

by

Kevin Gaspard  
Zhongjie Zhang  
Gavin Gautreau  
Murad Abufarsakh  
Mark Martinez

Louisiana Transportation Research Center  
4101 Gourrier Ave.  
Baton Rouge, LA 70808

LTRC Project No. 12-1P  
SIO No. 30000607

conducted for

Louisiana Department of Transportation and Development  
Louisiana Transportation Research Center

The contents of this report reflect the views of the author/principal investigator who is responsible for the facts and the accuracy of the data presented herein. The contents do not necessarily reflect the views or policies of the Louisiana Department of Transportation and Development the Federal Highway Administration or the Louisiana Transportation Research Center. This report does not constitute a standard, specification, or regulation.

May 2019



## ABSTRACT

LTRC has conducted a research study on LA 493 that provides evidence of damage to roadways caused by inundation. The evidence supporting this comes from three sources: a rod and level cross-section survey taken approximately one month prior to the first inundation event and subsequent cross-section surveys taken after the first to third inundation events; from pavement assessments with LTRC's profiler in June 2017 and June 2018; and from a structural assessment with the falling weight deflectometer (FWD).

Differential movements of the roadway surface were measured after the inundation events. The elevation increase at the centerline of the test sites varied from 2.44 mm to 44.5 mm after the first inundation event. Movements such as those measured will adversely affect the pavements performance leading to a reduced service life.

Results from the IRI testing implied that (1) there were high degrees of differential profile changes in the roadway surface, (2) the IRI was significantly higher than it should have been for a roadway with its service age, and (3) there was a high degree of IRI variation amongst the test sites. Data from rutting tests also had high degrees of variability. The maximum measured rut depth was 1.685 in.

Longitudinal crack data implied that (1) most of the sites had excessive longitudinal cracking for the time that they were in service, (2) the longitudinal cracking observed is consistent with volumetric changes occurring in the subgrade, and (3) it is logical to infer that the inundation events were responsible for both the magnitude and premature emergence of these longitudinal cracks.

Data from the FWD testing implied that structural damage was present. The amount of damage present ranged from 0.2 to 2.61 in. of equivalent asphaltic concrete thickness.

## **ACKNOWLEDGMENTS**

Significant contributions to this study were performed by Mitch Terrell, Terrell Gorham, Benjamin Key, Renee Crosse, Preston Causey, and Hend Alyousey.

## **IMPLEMENTATION STATEMENT**

There have been several studies conducted in Louisiana and internationally that demonstrated how the inundation of roadways causes structural damage. It would be beneficial to definitively discover the damage to the roadways with preflood and postflood data. DOTD can identify flood-prone roadways, and conduct structural testing either annually or biennially so as to create a database of the structural conditions of these roadways.



## TABLE OF CONTENTS

ABSTRACT.....	v
ACKNOWLEDGMENTS .....	vi
IMPLEMENTATION STATEMENT .....	vii
TABLE OF CONTENTS.....	ix
LIST OF TABLES .....	xi
LIST OF FIGURES .....	xii
INTRODUCTION .....	1
Literature Review.....	2
Assessments of Inundated Pavement Structures.....	2
Soil Physics and Seasonal Volumetric Change .....	10
Inundation .....	15
OBJECTIVE .....	17
SCOPE .....	19
METHODOLOGY .....	21
Experiment Design.....	21
Soil Classifications.....	22
Cross-section Survey Locations and Dates.....	23
Roadway Profiling and Imaging .....	24
Falling Weight Deflectometer.....	25
Data analysis and statistical testing.....	25
DISCUSSION OF RESULTS .....	27
Cross-section Survey .....	27
Site 1A Cross-section Results.....	27
Site 1 Cross-section Results.....	30
Site 2 Cross-section Results.....	32
Site 3 Cross-section Results.....	34
Site 4 Cross-section Results.....	36
Site 5 Cross-section Results.....	38
Site 6 Cross-section Results.....	40
Roadway profiling and imaging.....	42
IRI.....	42
Rutting.....	46
Maximum Rutting EB.....	49
Maximum Rutting WB .....	50
Longitudinal Cracking .....	51

Falling Weight Deflectometer.....	54
Structural Number.....	54
Subgrade Resilient Modulus.....	55
CONCLUSIONS.....	57
RECOMMENDATIONS.....	59
ACRONYMS, ABBREVIATIONS, AND SYMBOLS.....	61
REFERENCES.....	63
APPENDIX A.....	69
APPENDIX B.....	71

## LIST OF TABLES

Table 1 Experimental test sites .....	21
Table 2 Soil classifications .....	22
Table 3 Cross-section locations .....	23
Table 4 Cross-section survey dates .....	23
Table 5 Cross-section data for Site 1A .....	28
Table 6 Changes in cross-section elevations from 12/7/2015 for Site 1A.....	28
Table 7 Cross-section data for Site 1 .....	30
Table 8 Changes in cross-section elevations from 12/7/2015 for Site 1.....	31
Table 9 Cross-section data for Site 2 .....	33
Table 10 Changes in cross-section elevations from 12/7/2015 for Site 2.....	33
Table 11 Cross-section data for Site 3 .....	35
Table 12 Changes in cross-section elevations from 12/7/2015 for Site 3.....	35
Table 13 Cross-section data for Site 4 .....	37
Table 14 Changes in cross-section elevations from 12/7/2015 for Site 4.....	37
Table 15 Cross-section data for Site 5 .....	39
Table 16 Changes in cross-section elevations from 12/7/2015 for Site 5.....	39
Table 17 Cross-section data for Site 6 .....	41
Table 18 Changes in cross-section elevations from 12/7/2015 for site 6 .....	41
Table 19 EB and WB descriptive statistical IRI data for the June 2017 assessment.....	43
Table 20 IRI statistical results for the June 2018 assessment.....	45
Table 21 Rutting statistical results for the June 2017 assessment .....	47
Table 22 Rutting statistical results for the June 2018 assessment .....	48
Table 23 Overall rutting statistical results .....	49
Table 24 Longitudinal cracking statistical analysis for June 2017 .....	53
Table 25 Longitudinal cracking statistical analysis for June 2018 .....	53
Table 26 Overall statistical grouping for longitudinal cracks.....	54
Table 27 $SN_{eff}$ and damage statistical results for the June 2018 assessment.....	55
Table 28 Subgrade $M_r$ statistical results .....	56

## LIST OF FIGURES

Figure 1 Longitudinal cracks: LA 1200: CSLM 2.348.....	11
Figure 2 Multiple longitudinal cracks: La 494: CSLM 1.864 .....	11
Figure 3 Effect of moisture change on pavement structure .....	12
Figure 4 Alligator cracking in AC surface.....	12
Figure 5 Parish road: St. Martin Parish.....	13
Figure 6 Permanent desiccation: Source Roberts [48] .....	14
Figure 7 Multiple longitudinal cracks and subsidence: West Parker Ave. near LTRC .....	14
Figure 8 Dynamic settlement: Source Biddle [47] .....	15
Figure 9 Volumetric moisture content versus void ratio .....	16
Figure 10 Aerial view of LA 493 test site locations .....	21
Figure 11 Cross-section point locations.....	24
Figure 12 Charts of cross-section points for Site 1A .....	29
Figure 13 Charts of cross-section points for Site 1A.....	29
Figure 14 Charts of cross-section points for Site 1 .....	31
Figure 15 Charts of cross-section points for Site 1 .....	32
Figure 16 Charts of cross-sections for Site 2 .....	33
Figure 17 Charts of cross-sections elevations from 12/7/2015 for Site 2.....	34
Figure 18 Charts of cross-section points for Site 3.....	35
Figure 19 Charts of cross-section points for Site 3.....	36
Figure 20 Charts of cross-section points for Site 4.....	37
Figure 21 Charts of cross-section points for Site 4.....	38
Figure 22 Charts of cross-section points for Site 5.....	39
Figure 23 Charts of cross-section points for Site 5.....	40
Figure 24 Charts of cross-section points for Site 6.....	41
Figure 25 Charts of cross-section points for Site 6.....	42
Figure 26 EB and WB IRI values for the June 2017 assessment.....	44
Figure 27 EB and WB IRI values for the June 2018 assessment.....	46
Figure 28 EB maximum rutting for Sites 1 to 4.....	50
Figure 29 EB maximum rutting for Sites 5 and 6.....	50
Figure 30 WB maximum rutting for Sites 1 to 4 .....	51
Figure 31 WB maximum rutting for Sites 5 and 6.....	51
Figure 32 Longitudinal cracks for the EB and EB directions for the June 2017 and June 2018 assessments.....	54
Figure 33 LA 493 title sheet .....	69
Figure 34 Typical section for Site 1.....	71

Figure 35 Typical section for Site 2.....	72
Figure 36 Typical section for Site 3.....	73
Figure 37 Typical section for Site 4.....	74
Figure 38 Typical section for Site 5.....	75
Figure 39 Typical section for Site 6.....	76



## INTRODUCTION

According to the National Oceanic and Atmospheric Administration (NOAA), there have been 233 weather and climatic disasters exceeding \$1 billion per event in the USA between 1980 and 2018 [1]. It is estimated that the total costs of these events exceeds \$1.5 trillion dollars [1-2]. As of April 30, 2018, the Federal Emergency Management Administration (FEMA) has reported that there have been 118 significant flooding events since 1978 in the USA, costing over \$57 billion [3]. Eleven (9.3 percent) of these significant flooding events have occurred in Louisiana [3].

There is a plethora of publications providing predictions of continual extreme weather events that will ultimately lead to more severe flooding or inundation events [4-5]. It is imperative that DOTD establish pavement management and engineering methods to address future inundation events. This report focuses on assessing the damage to roadway pavements caused by inundation.

The Louisiana Transportation Research Center (LTRC) conducted a research project to determine the damage caused by trees on roadway pavement structures [6-7]. The experimental sites were constructed on Louisiana Highway 493 in Natchitoches Parish under State Project H.011071 as presented in Appendix A. It is a rural highway with a current average daily traffic of 330 with 12 percent trucks.

LTRC's experiment design was based upon assessing the normal seasonal variation properties of the pavement layers for LA 493. Unfortunately, within approximately two months after the newly constructed roadway was fully opened to traffic, it was inundated for several months (January 2016 to March 2016) due to a heavy rainfall event. Since that time it was inundated twice more: February 2017 to April 2017 and July 2017 to August 2017. Inundation events created higher soil saturation events beyond the normal seasonal variation in the soil and base course layers based upon LTRC's knowledge. Therefore, the objectives and scope of the original experiment design were modified to determine the impact of the inundation events.

The damage to a newly constructed pavement caused by the inundation events was catalogued from December 2015 to July 2018. Evidence of the pavement damage will be illustrated using data from a cross-section survey conducted in December 2015 approximately one month prior to the first inundation event (January 2016 to March 2016). Subsequent cross-section surveys were conducted and the results from the cross-section

surveys will be presented later in this paper. The pavement surface was assessed using the LTRC profiling and imaging vehicle (profiler) as well as its falling weight deflectometer (FWD) discussed in detail later.

## **Literature Review**

### **Assessments of Inundated Pavement Structures**

On August 29, 2005, Hurricane Katrina devastated New Orleans and southeastern Louisiana, leaving hundreds of thousands either displaced or homeless. Nearly four weeks later, Hurricane Rita made landfall in the southwestern portion of the State, further damaging Louisiana's infrastructure and impacting the New Orleans area once again [8-9].

LTRC conducted a research project to assess the damage caused to DOTD roadways in New Orleans, St. Bernard, and Jefferson parishes [8-9]. Approximately 235 miles of roadways {asphaltic concrete (AC), composite, and portland cement concrete (PCC)} were tested with the falling weight deflectometer (FWD), ground penetrating radar (GPR), and dynamic cone penetrometer (DCP). Coring of the roadway was also performed to validate GPR readings as well as determine the type and thickness of the pavement and base course. The soil type was determined using visual inspection from the cores. A typical forensic approach of comparing "before and after" flooding structural conditions could not be conducted on the tested roadways with the exception of one roadway, LA 46. Prior to the flood, LTRC had conducted a forensic analysis on LA 46. Comparing the strength of LA 46 before and after the flooding indicated that the damage to its structure was equivalent to approximately 3 in. of AC.

In order to conduct a statistical analysis, the pavements were stratified according their type (AC, composite, and PCC), and flooding condition (flooded, non-flooded). From there, they were further stratified based upon depth of inundation, duration of inundation, and pavement thickness. Though there was some variance in the structural damage amongst the groups, all groups generally produced results that confirmed the non-flooded pavements were stronger than the flooded pavements.

Depending upon the data groups, the amount of AC required to mitigate damages to the AC pavements ranged from 0.59 to 3.57 in., composite pavements ranged from 0 to 3.27 in., and PCC pavements ranged from 0 to 1.18 in. It should be noted that these results were based upon a network analysis, and some roadways may actually need more AC to mitigate the damages. This could only be determined by a project based analysis, which was beyond the

scope of this study. Furthermore, the amount of asphalt (3 in.) determined from the “before and after” analysis for LA 46 falls within the range for composite pavements (0 to 3.27 in.) as determined by the spatial analysis [8-9].

Stantec Consultant Services conducted a study in 2015, which was not published, for the City of New Orleans entitled, “Quantification of Flood Damage from Hurricane Katrina on the City of New Orleans Pavement Network.” Three-hundred and ten miles of roadways (20 percent of their network) were selected using statistical sampling for assessment with the FWD, GPR, profiler-imaging vehicle, and coring. The streets were stratified into four groups: network level, neighborhood level, street level and roadway level. Four major parameters were assigned to the streets in each of the groups previously listed: flood condition, pavement type, subgrade type, and functional class.

The variables used to catalogue the pavement conditions were IRI, pavement quality index, surface distresses, subgrade resilient modulus ( $M_r$ ), modulus of subgrade reaction ( $k$ ), in-place structural number ( $SN_{eff}$ ), and effective slab thickness ( $D_{eff}$ ). Stantec used a weighted approach to demonstrate the damage caused by the flooding and debris hauling. For AC and composite pavements, they concluded that the damage was equivalent to 1.21 SN or 2.9 in. AC whereas the damage to PCC roads was equivalent 0.51 in.  $D_{eff}$  or 0.51 in. PCC.

Helali et.al. conducted a study for Jefferson Parish in Louisiana [10]. Twenty percent (338 miles) of roadways in their network were selected for assessment using statistical sampling methods. The parameters used in their analysis were flooding condition (flooded versus non-flooded), traffic levels, subgrade soil type, jurisdiction, and availability of historical data. Distress data was collected with their profiler-imaging vehicle and FWD.

The results of their network level analysis concluded that the flooded pavements were in significantly worse condition than the non-flooded pavements. For AC pavements, the difference in strengths were on average equivalent to 1 SN or 2.3 in. AC. Regarding PCC, the average difference  $D_{eff}$  was 0.92 which is equivalent to 0.92 in. PCC.

Vennapusa et.al. conducted a study to capture the damage caused by flooding from the Missouri River in Iowa [11]. The estimated damage was \$63 million to primary and secondary roadways in the counties studied. Roadway testing was conducted with the FWD, DCP, GPR, 3-D laser scanning, and hand auger borings. Assessments were conducted on roadways with gravel, AC, chip sealed, and PCC surfaces.

On gravel roads, results from FWD testing indicated that the flooded gravel roads were significantly weaker than the non-flooded roads based upon the statistical analysis [11]. The results also indicated that the subgrade had an 86 percent influence on the FWD measurements while the gravel had approximately a 14 percent influence. This was a significant finding in that the response to dynamic loading due to traffic will be highly dependent on the quality of the subgrade soil. Rutting of up to 4.9 in. deep was observed in some locations. Those locations had California bearing ratio (CBR) readings of less than 2.

Only one AC pavement was tested, an AC thickness of 14 in. and the base course thickness was 12 inches [11]. The modulus of the AC and subgrade obtained from the FWD were approximately 1.35 times higher in the non-flooded area as compared to the flooded area 6 months after the flooding event. FWD readings taken 9 months after the flooding event showed similar modulus values between the flooded and non-flooded areas. The CBR values in the subgrade were around 10 times higher in the non-flooded areas relative the flood area. No structural failures were noted on the pavement, but erosion of the granular shoulder in regions near the high water line was observed.

As with the AC pavement, only one PCC pavement was tested, with a PCC pavement thickness of 9.8 in. and a 6 in. thick base course [11]. This section of roadway was subjected to rapid water currents which eroded some of the base course and embankment beneath the pavement. The voids were filled with flowable cement grout. Longitudinal cracks were observed in some panels where the base course had been removed due to erosion. Load transfer efficiency (LTE) ranged from 93 to 95 percent during testing. The  $k_{static}$  values varied from 55 to 73 psi which rated poor [12]. The CBR values were 20 on average in the top 12 in. of the subgrade.

Sultana et. al. conducted a study to evaluate the effects of flooding from an extreme weather event (January 2011) that occurred in South-East Queensland [13]. The study was initiated by Austroads in 2013. Between the periods of 1967 to 2005, the direct damage due to floods was approximately \$377 million Australian dollars per year. The total damage to the public infrastructure was estimated to range from \$5 to \$6 billion Australian dollars. Data was collected using an FWD on flooded and non-flooded roads. The data was used to calculate the layer moduli and CBR value for the subgrade. With that data, the modified structural number was calculated using equation (1) [14].

$$SNC_i = 3.2 \times D_0^{-0.63} \quad (1)$$

where,

$SNC_i$  = modified structural number at age 'i'

$D_0$  = maximum deflection (mm) at load center at age 'i'

Network level structural deterioration models for AC pavements {equation (2)} and sealed unbound granular pavements {equation (3)} were also used in their comparisons of flooded to non-flooded pavements [15].

$$SNC_{ratio} = 0.991*(2 - EXP(0.00132 \times TMI_i + 0.256*(AGE_i / DL)) \quad (2)$$

$$SNC_{ratio} = 0.9035*(2 - EXP(0.0023 \times TMI_i + 0.1849*(AGE_i / DL)) \quad (3)$$

where,

$SNC_{ratio}$  = current strength of pavement/subgrade relative to its initial strength (=  $SNC_i / SNC_0$ ).

$SNC_i$  = modified structural number at the time 'i' of measurement.

$SNC_0$  = modified structural number at the time 'i' of pavement construction.

$TMI_i$  = Thornthwaite Moisture Index at the time 'i' of measurement.

$AGE_i$  = age of pavement (number of years since construction or last rehabilitation).

$DL$  = pavement design life (years)

After conducting a detailed statistical analysis comparing flooded roads to non-flooded roads, Sultana et. al. concluded that flooding caused up to a 50 percent decrease in structural number and that the subgrade CBR was reduced up to 67 percent as well.

Alam and Zakaria published a paper discussing the detrimental impact of perennial floods on the infrastructure of Bangladesh [16]. They noted two primary categories of damage to roadways: embankment slope failures and pavement failures. They conducted a parametric study using CBR tests from subgrade soil samples and Marshall stability and flow tests from AC pavement samples.

CBR tests were conducted on specimens at three compaction levels: 56 blows, 35 blows, and 10 blows. The specimens from the three compactive levels were submerged in water for 4, 7, 30, and 45 days. The four, day soak period was used as the control due to the fact that CBR values are normally determined after soaking the samples in water for four days. The reduction in CBR values (relative to the control) were 16.7, 29.6, and 37.5 percent for the 56, 35, and 10 blow specimens, respectively.

AC specimens were prepared in the laboratory with an asphalt content of 4.75 percent. Four sets of samples were prepared and submerged in water for 4, 7, and 30 days with alternating drying and wetting cycles. Marshall stability and flow tests were performed on the samples. Based upon the test results, the flow of the AC mixture increased by 35, 50, and 93 percent for the 4, 7, and 30 day submerged samples. Regarding the stability of the AC, it decreased by 13, 19, and 26 percent for the 4, 7, and 30 day specimens.

The results of this laboratory experiment demonstrates the adverse effects that occur to both the AC pavement and subgrade when they are submerged for extended periods of time.

Mallick et.al. conducted a study where “systems dynamics” was used to create a software package that calculated the critical time ( $T_{critical}$ ) for AC pavement and unbound base course required to reach failure due to inundation [17-20]. Water entry into the AC pavement and underlying base course was calculated by modifying the Green and Ampt water infiltration equation [21]. The equation originally was developed to estimate the infiltration of water into soil as presented in equation (4). Mallick et.al. modified the equation to take into account the time required for water to infiltrate the AC pavement as presented in equation (5) [17].

$$t = ((\theta_s - \theta_i) / k_{effective}) * [L_f - (h_L - \Psi_f) * \ln((h_L + L_f - \Psi_f) / (h_L - \Psi_f))] \quad (4)$$

where,

$\theta_s$  = volumetric moisture content at saturation.

$\theta_i$  = initial volumetric moisture content.

$L_f$  = thickness of (AC+base course), m.

$\Psi_f$  = suction, m.

$h_L$  = depth of ponded water, m.

$t$  = time to infiltrate, m/s.

$k_{effective}$  = permeability, m/s.

$$k_{effective} = (h_{AC} + h_{base}) / ((h_{AC}/k_{AC}) + (h_{base}/k_{base})) \quad (5)$$

where,

$h_{AC}$  = thickness of AC, m.

$h_{base}$  = thickness of unbound base course, m.

$k_{AC}$  = permeability of AC, m/s.

$k_{base}$  = permeability of base course, m/s.

The systems dynamic model also included equations to take into account base course erosion if the pavement was near a stream and the reduction in tensile strength of the AC pavement due to inundation as presented in equations (6) and (7) [22-23].

$$V_c = 0.35 * D_{50}^{0.45} \quad (6)$$

where,

$V_c$  = critical flow velocity (m/s).

$D_{50}$  = particle size medium diameter (mm).

$$RTS(t) = RTS(i) - RRTS * t \quad (7)$$

where,

$RTS(t)$  = retained tensile strength at any time  $t$ , %

$RTS(i)$  = initial tensile strength (at construction), %

$RRTS$  = rate of change (deterioration) in retained tensile strength, % per unit of time (years)

$t$  = time at which the retained tensile strength is determined, years.

The results of their simulations using the systems dynamic approach indicated that the model was sensitive to (1) length of inundation period, (2) distress condition of the AC pavement and base course at the time of inundation, (3) thickness of AC pavement and base course, and (4) permeability of AC pavement and base course. The authors pointed out that the model could be improved with further research. The model can be used as a risk analysis tool for flood prone pavements.

Khan et.al. conducted a series of studies where road deterioration (RD) models were developed for the parameters of rutting and IRI for inundated roads in Queensland, Australia [24-28]. The latest generation of models included performance models based upon the probability ( $P_r$ ) of flooding, period of flooding, and loss of subgrade resilient modulus ( $M_rL$ ) due to flooding. Khan et.al. discovered in their analyses that the gradient changes of rutting produced similar results to that of IRI [24]. Because of that, models for rutting were not provided. The two new gradients proposed were  $\Delta IRI/P_r$  and  $\Delta IRI/M_rL$ .

Monte Carlo simulations were used to test the new gradients. Simulations included (1) varying probabilities of flooding, (2) proposed  $\Delta IRI/P_r$ , (3) proposed  $\Delta IRI/M_rL$ , and (4) consequences of flooding. The results indicated that the models provided useful knowledge on the consequences of flooding for various types of sections. PCC and robust AC

pavements were discovered to be the most flood resilient, which was consistent with the published literature [6-13]. The simulations indicated that the pavements with the poorest performance had the highest risk of flood probabilities. The advantage of the developed Monte Carlo models for  $\Delta\text{IRI}/P_r$  and  $\Delta\text{IRI}/M_rL$  is that it allows agencies to assess their pavements prior to flooding events and take action to minimize the risks.

Sultana et.al conducted a state of the art literature review seeking to discover publications on the effects of flooding on roadway infrastructures [29]. Based upon their discoveries as well as research they conducted for others, they developed two mechanistic-empirical-deterministic deterioration models to predict rutting and roughness of flooded pavements [29-31]. They postulated that more effective decisions can be made regarding pavement rehabilitation based upon their models.

The model developed for rutting is presented in equation (8). It is a function of the time lapse between data acquired after flooding and prior to flooding. This model had a pearson correlation coefficient  $r^2$  of 0.67 and a sample size (n) of 436.

$$\Delta\text{Rut}_{\text{post-flood}} = k_{\text{rut}} \times [(0.083 \times t^{0.85}) + (0.109 \times \text{Rut}_{\text{pre-flood}}) - 0.746] \quad (8)$$

where,

$\Delta\text{Rut}_{\text{post-flood}}$  = difference in pre-flood and post-flood rutting (mm).

$k_{\text{rut}}$  = local calibration for rutting (dimensionless)

$t$  = time lapse in rutting in days after flood ( $t < 172$  days)

$\text{Rut}_{\text{pre-flood}}$  = pre-flood rutting (mm).

The roughness model is presented in equation (9). It is also a function of the time lapse between data acquired after flooding and prior to flooding. This model had a pearson correlation coefficient ( $r^2$ ) of 0.319 and a sample size (n) of 436.

$$\Delta\text{IRI}_{\text{post-flood}} = k_{\text{rg}} \times [0.039 + (0.027 \times t^{0.5})] \quad (9)$$

where,

$\Delta\text{IRI}_{\text{post-flood}}$  = difference in pre-flood and post-flood IRI (m/km).

$k_{\text{rg}}$  = local calibration for IRI (dimensionless)

$t$  = time lapse in IRI in days after flood ( $t < 172$  days)

Shamsabadi et.al. conducted a study to determine the effects of snow storms and flooding events on the performance of highway pavements [32]. They did so by extracting pavement data from the Long Term Pavement Performance (LTPP) program and climate data from the NOAA database. The datasets used were from four states and covered a period of 17 years. Equation (10) presents the flexible pavement model developed for areas affected by snow storms, freeze thaw events, and large precipitation events developed by Jackson et.al. [33].

$$\ln(\Delta\text{IRI}+1) = \text{Age}(4.5\text{FI} + 1.78\text{CI} + 1.09\text{FTC} + 2.4\text{PRECIP} + 5.39\log(\text{ESAL}) / \text{SN} \quad (10)$$

where,

$\Delta\text{IRI}$  = change in International roughness index (m/km).

Age = pavement age (years).

FI = freezing index (degree-days when air temperatures are below and above zero degrees Celsius).

CI = cooling index (temperature relation to the relative humidity and discomfort).

FTC – freeze-thaw cycle.

PRECIP = precipitation.

ESAL = equivalent single axle load.

SN = structural number.

Equation (10) was further refined by Shamsabadi et.al. as presented in equation (11). The authors wrote that the deterioration model could result in more realistic assessments of future costs, maintenance planning, and rehabilitation activities.

$$\% \Delta\text{IRI} = 5.09 - 2.5\text{NIRI} + 1.7\text{NDepth} - 1.74\text{NDuration} + 0.706\text{ESAL} * \text{NDuration} \quad (11)$$

where,

$\% \Delta\text{IRI}$  = Percentage increase in IRI due to the snow storm.

NIRI = Normalized IRI of the section before the snow storm.

NDepth = Normalized depth of the snow storm.

NDuration = Normalized duration of the snow storm.

ESAL = equivalent single axle load (derived from traffic).

Elshaer assessed the mechanical responses of pavements during and after flooding in part by using models developed for the Mechanistic Empirical Design Pavement Guide (MEPDG) [34-35]. Elshaer used layered elastic methods to conduct the analyses in his dissertation. The objectives were to (1) determine analysis methods to evaluate post-flood pavements, (2)

determine the performance of flooded pavements, (3) significant parameters to obtain following a flooding event, (4) develop a state of the art method to incorporate subgrade soil moisture into the analysis, (5) enhance knowledge on the effect of subsurface water on the load carrying capacity of pavements, (6) determine the stress dependency and moisture sensitivity of unbound materials, (7) the effect of suction and the resilient behavior on unbound materials, and (8) provide procedures to determine the failure time of flooded pavements.

The major conclusions derived from the research were, (1) incorporating the effects of suction into the analysis influenced the performance predictions, (2) the load carrying capacity is greater in coarse grain soils than fine grain soils, (3) the depth of the water table is more significant upon pavement performance for fine grain soils than coarse grain soils, and (4) load distribution from the tires to the pavement structure differ significantly as the water table returns to its pre-flood depth. The contents of this study establishes a framework that requires further validation using a wider variety of soils types as well as field validation.

### **Soil Physics and Seasonal Volumetric Change**

Pavement surface and embankment distresses due to seasonal moisture variation in the base course, subgrade, foreslope, ditches, and backslope are both a national and international issue existing since the first hard surfaced pavements were constructed [36-43]. Clay soils, which are prevalent in some regions of Louisiana, can be particularly vulnerable to changes in moisture content, shrinking during drying (desiccation) and swelling during wetting (absorption). In some instances, soils with high silt contents may also exhibit volume changes and desiccation cracking. Volume changes and/or tension cracks can be accelerated or increased when trees are present. Trees extract water from the soil, which in turn increases the suction stresses in the soil as well as the magnitude of moisture content changes due to the seasonal wetting and drying the embankment soil and base course.

In Louisiana, it is LTRC's opinion that a proportion of longitudinal cracks, meandering cracks, subsidence, and heaving, in the pavement layers have occurred as a result of seasonal volume changes in the roadway embankment. In some instances, trees are present, further adding to the distresses previously mentioned as presented in Figures 1 and 2. Distresses and volume changes have and will continue to lead to pavement service life reduction, costly maintenance repairs, and complaints from the public.



**Figure 1**  
**Longitudinal cracks: LA 1200: CSLM 2.348**



**Figure 2**  
**Multiple longitudinal cracks: La 494: CSLM 1.864**

Pavement surface distresses resulting from seasonal soil moisture content variation can be attributed to four major factors as well as their interactions:

1. Transverse and longitudinal volumetric change differential (due to wetting and drying) in the embankment, base course, and adjacent natural ground.
2. Desiccation cracking.
3. Dynamic settlement due to soil densification caused by soil suction stresses.
4. Slope failures.

Volumetric changes in the subgrade and/or base course differ in the travel lane(s) in that the volume change at the center line of the pavement differs significantly from the volume change at the pavement edge. Near the pavement edge, movement may be significant enough to cause damage as presented in Figure 3. Such a volumetric differential can manifest either as single or multiple longitudinal crack(s) beginning approximately 1 to 3 ft. from the pavement edge due to pavement bending (heave and subsidence) as presented in Figures 1, 2, and 3 [42-46]. As a result of continual bending, alligator cracking patterns have been known to occur in the asphaltic (AC) surface as presented in Figure 4. The volume change also occurs longitudinally along the travel lane(s) which can lead to bumps and depressions in the pavement. This in turn contributes to decreased ride quality due to the changes in the roadway profile.

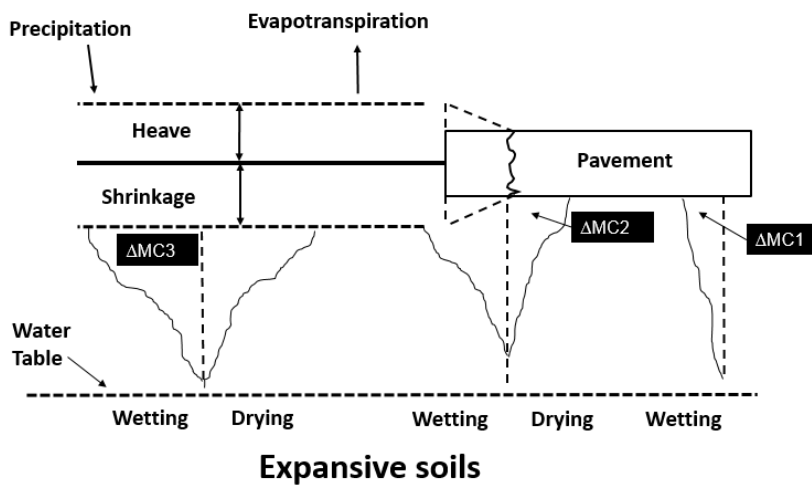


**Figure 3**  
Effect of moisture change on pavement structure



**Figure 4**  
Alligator cracking in AC surface

Longitudinal cracks in the pavement may also be caused by desiccation in the expansive clay subgrade. When the soil suction stresses induced by desiccation coupled with net normal

stress exceed the tensile strength of the soil, a crack will form as shown in Figure 5 [39-41]. When this occurs beneath the pavement, it is possible for the crack to propagate through the pavement structure as presented in Figures 1 to 3.



**Figure 5**  
**Parish road: St. Martin Parish**

While it is possible for desiccation to be completely driven by evaporation alone, the presence of flora accelerates the process through transpiration. Transpiration is the passage of water through a plant or tree from its roots through its vascular system to the atmosphere by way of the leaves [36, 47-49]. The transpiration period for trees typically begins during the spring and peaks during the summer months, which adds to the desiccation caused by evaporation. The process of evaporation and transpiration together is called evapotranspiration [36].

When the yearly rainfall is insufficient to return the active zone (the depth of soil layer(s) impacted by evapotranspiration) to its field capacity (equilibrium saturation), a zone of permanent desiccation is created as presented in Figure 6 [36-38, 47,48]. If permanent desiccation occurs either near the pavement edge or beneath it, permanent settlement (dynamic settlement) at that location may be the culprit of both multiple longitudinal cracks and subsidence as shown in Figures 1, 2, 6, 7, and 8 [47].

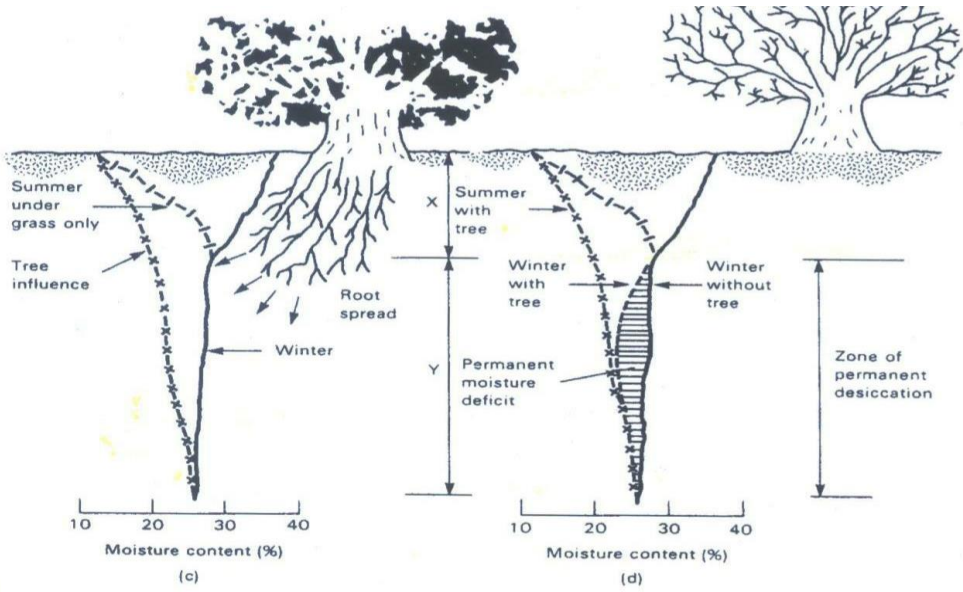


**Figure 6**  
**Permanent desiccation: Source Roberts [48]**



**Figure 7**  
**Multiple longitudinal cracks and subsidence: West Parker Ave. near LTRC**

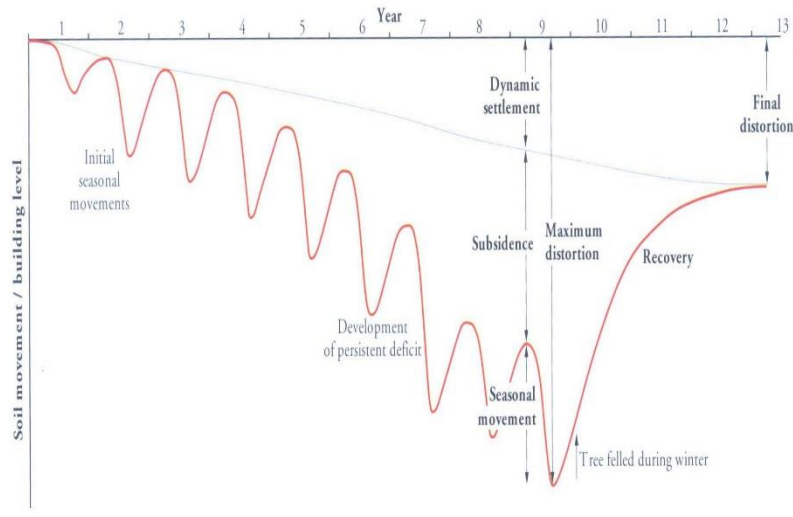


Figure 7.7

**Figure 8**  
**Dynamic settlement: Source Biddle [47]**

Slope failures may also occur due to seasonal moisture variation. If tension cracks develop in the embankment slope during desiccation, a failure plane may develop. Tension cracks create direct paths for water infiltration. This can quickly saturate the embankment reducing its shear strength which can lead to failure. Cracks as deep as 3 ft. and as wide as 2.5 in. have been measured by LTRC as presented in Figure 5. These cracks are probably due to a combination of distress mechanisms such as volumetric changes, desiccation cracking, and slope failures.

### **Inundation**

The pavement distress and soil physics phenomenon previously described were intended to illustrate what happens during normal seasonal wetting and drying events. Inundation of the roadway serves to exacerbate the swelling and shrinking of expansive soils by fully saturating (100 percent) the soil and base course.

For example, let's assume that the volumetric moisture content (VMC) beneath the pavement ( $\Delta MC1$ ) normally ranges from 65 to 85 percent, and the VMC at the edge of the pavement ( $\Delta MC2$ ) normally ranges from 35 to 65 percent while the VMC at a location away from the pavement ( $\Delta MC3$ ) (natural ground) ranges from 15 to 55 percent seasonally; refer to Figure 3.

After an inundation event, it is possible and probable for the soil to fully saturate (VMC = 100 percent) at  $\Delta MC1$ ,  $\Delta MC2$ , and  $\Delta MC3$ . Once the flood waters recede and the roadway, embankment, and natural ground become exposed to the atmosphere and sunlight, evaporation will occur. If it is in the spring and summer, evaporation will be even greater where trees are present due the transpiration of the trees and other flora. So instead of  $\Delta MC1$ ,  $\Delta MC2$ , and  $\Delta MC3$  ranging from their normal VMC maximums of 85 percent, 65 percent, and 55 percent, they now range respectively from 100 percent to 65 percent, 100 percent to 35 percent, and 100 percent to 15 percent. Such changes in the VMC in an expansive soil will increase the magnitude of its swell, thus, leading to a larger range of ground movement due to swell. Furthermore, as evaporation and transportation remove water from the ground and beneath the pavement surface, shrinkage will occur leading to subsidence in the ground. However, under this circumstance, the range between swelling and shrinking is greater than the normal range experienced for this area under normal seasonal variation. Such a range in movement can damage the pavement leading to premature failures and cracking with subsequent service life reductions. Figure 9 presents the general relationship of void ratio ( $e$ ) versus VMC for an expansive soil. Through formulas, the volume change and subsequent change in height or ground movement can be calculated. As the soil varies in its mineralogical composition, so will the relationship between void ratio and VMC [39-41].

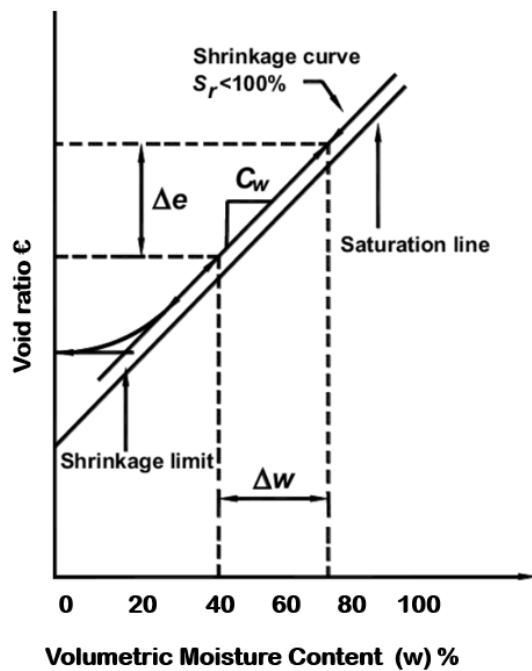


**Figure 9**  
**Volumetric moisture content versus void ratio**

## **OBJECTIVE**

The objectives of this study were to measure the seasonal pavement surface movements, the impact of inundation on the functional properties of the pavement structure, and the impact of inundation on the structural properties of the pavement structure.



## **SCOPE**

This report covers the impact of inundation on the six test sites on LA 493. The effects of inundation were measured by conducting cross-section surveys on the six sites between December 2015 to March 2018. The functional properties of the pavement surface were determined with LTRC's profiler and imaging system. From this, the IRI, rutting, and surface cracking were measured on assessments in June 2017 and June 2018. The structural properties were measured with the FWD in July 2018. The data was used to calculate the in-place structural number and subgrade resilient modulus.



# METHODOLOGY

## Experiment Design

The test sites were constructed on LA 493 in Natchitoches Parish; refer to Appendix A. Test site treatments varied in thickness and type as presented in Table 1. They were initially designed to discover the effectiveness of the treatments on mitigating pavement distresses caused by normal seasonal volumetric changes in expansive clays when trees are located at the right- of-way line as presented in Figure 10. Figures for the typical sections of the test sites can be found in Appendix B.

**Table 1**  
**Experimental test sites**

Test Site Number	Notes	Additional Treatments	Stations			Typical Section Layers (in.)								
			From	To	Length (ft.)	AC	AST	SC	Stone	Geogrid	Geosynthetic Fabric	Sand Layer	Select Material	Lime Treated
1A	No Trees		10+00	12+00	200	3.5	Yes	8.5	No	No	Yes	12	3.5	No
1			12+00	18+00	600	3.5	Yes	8.5	No	No	Yes	12	3.5	No
2			18+00	25+00	700	3.5	No	8.5	4	No	Yes	No	12	12
3		Paved Foreslope of Embankment	25+00	32+00	700	3.5	Yes	8.5	No	No	Yes	No	12	12
4		Sand Basin in Ditch Bottom	33+02	41+02	800	3.5	Yes	8.5	No	No	Yes	No	12	12
5	Control Section Without Grid		41+02	49+02	800	3.5	Yes	8.5	No	No	Yes	No	12	12
6	Control Section With Grid		49+02	57+02	800	3.5	Yes	8.5	No	Yes	Yes	No	12	12

**Legend:** AC- asphaltic concrete; AST- asphalt surface treatment on soil cement; SC- soil cement base course; Stone- crushed stone base course interlayer; Select Material- soil that meets DOTD's usable soil criteria; Lime Treated - subgrade soil that was treated with lime.

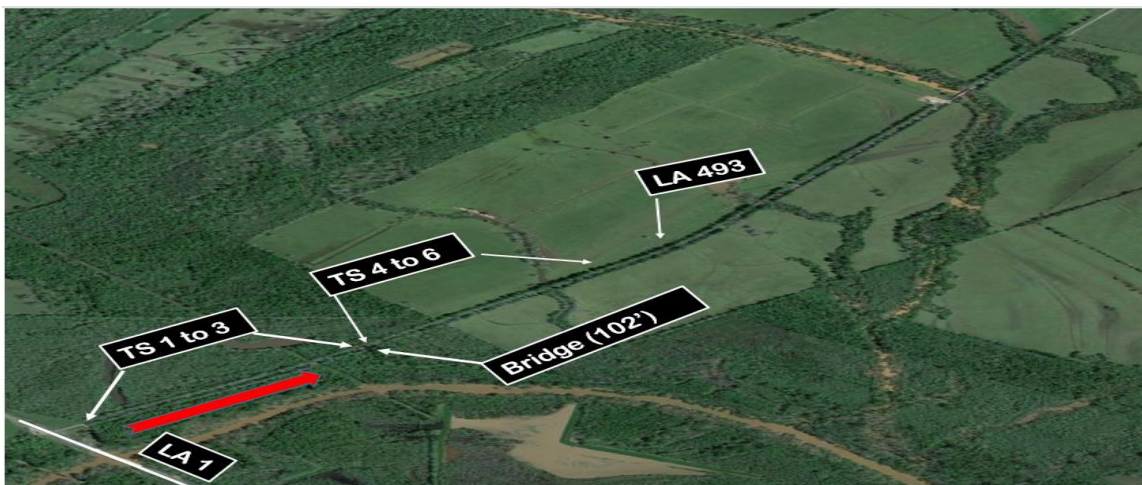


**Figure 10**  
**Aerial view of LA 493 test site locations**

Three inundation events so far have occurred after both lanes of the roadway were open to traffic in December 2015. The first inundation event occurred from approximately January 2016 to March 2016. Subsequent inundation events occurred on February 2017 to April 2017 and July 2017 to August 2017. These events negated the original intent previously discussed; but LTRC was able to develop a new experiment in which the effects of inundation could be investigated on the test sections constructed on this project which will be discussed later.

### Soil Classifications

During construction on this project, soil samples were taken in the test site locations as presented in Table 2. The results of the soil classification tests indicated that the untreated soil in the subgrade were clays with AASHTO classification types of either A-7(6) or A-7(5). Clays with liquid limits (LL) greater than 70 have severe swelling/shrinkage potential [36-40]. Rows in Table 2 with “lime” listed in them refer to the lime treated subgrade layer. The select material used on the project met DOTD’s usable soil criteria and classified as an A-6(4) while the sand used on the project classified as an A-3. The column labeled in-place moisture content refers to the gravimetric moisture content present in the soil when they were collected from the field.

**Table 2**  
**Soil classifications**

Test section & layer	AASHTO Type	USCS Type	In-place moisture content	Atterberg Limits %			Organic Content %
				LL	PL	PI	
			%				
Site 1 Subgrade	A-7(6)	CH	26.5	79	27	52	2
Site 3 Subgrade	A-7(6)	CH	25.1	76	25	51	1
Site 3 Lime	A-7(5)	CH	25.6	67	30	37	1
Site 4 Subgrade	A-7(5)	CH	14.0	64	24	40	1
Site 4 Lime	A-7(6)	CL	18.3	42	28	14	1
Site 5 Subgrade	A-7(5)	CH	17.1	57	20	37	2
Site 5 Lime	A-4 (0)	SM	17.9	40	35	5	1
Select Material	A-6 (4)	CL	20.7	35	21	14	1
Sand	A-3 (0)	SW	4.7	22	22	0	0

**Note:** Lime - lime treated subgrade

### Cross-section Survey Locations and Dates

LTRC conducted cross-section surveys in each of the test sites at the locations and dates presented in Tables 3 and 4. Two locations were surveyed in test Site 1 because the first portion of the site (Station 10+00 to approximately Station 12+00) had no trees adjacent to the right-of-way and the second portion (Station 12+00 to Station 18+00) did. At the time of the first cross-section survey date (12-7-15), the roadway had been open to traffic for approximately 1 month and then flooded from approximately (January 2016 to March 2016). The level used for the cross-section survey was a Trimble digital level and readings were recorded at a vertical accuracy of 0.001 ft. (0.3048 mm). The bench mark used for the survey was the bridge concrete rail at Station 32+50 left of the centerline. All elevations in this report were assumed.

**Table 3**  
**Cross-section locations**

Test Site	Cross-section survey	Location (Station)	Trees Present
1	1A	10+75	No
	1	14+00	Yes
2	2	21+44	Yes
3	3	29+19	Yes
4	4	37+14	Yes
5	5	45+21	Yes
6	6	53+08	Yes

**Table 4**  
**Cross-section survey dates**

Cross-section survey dates (month-day-year)	Flooding Event (month - year)
12-7-2015	1-2016 to 3-2016
4-25-2016	2-2017 to 4-2017
6-16-2016	7-2017 to 8-2017
9-20-2016	
12-6-2016	
4-25-2017	
7-13-2017	
9-15-2017	
12-6-2017	
3-15-2018	

LTRC conducted cross-section surveys at the points on the roadway’s AC surface shown in Figure 11. Doing so provided insight on the magnitude of movement translating to the surface of the roadway due to inundation. Measurements, both vertical and horizontal, were converted and are presented in metric units (mm) for convenience purposes.

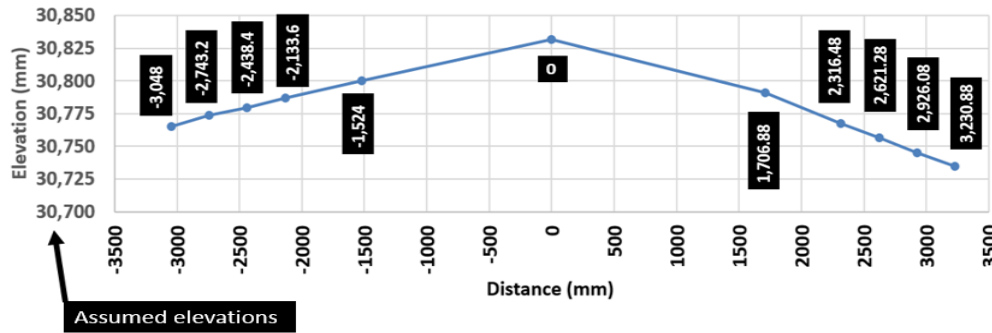


**Figure 11**  
**Cross-section point locations**

### Roadway Profiling and Imaging

LTRC’s roadway profiler and imaging vehicle, hereafter referred to as profiler, was used to assess the roadway surface in the test section locations [50]. LTRC’s profiler is specially designed in that it measures the roadway surface profile in the left wheel path (LWP), right wheel path (RWP) and in the center of the lane (CLP). It is LTRC’s experience that on typical roadways in Louisiana, both the LWP and RWP IRI measurements will be generally higher than the CLP measurements because the vehicle tires generally do not make contact with the center of the lane. In most cases, the IRI measurements from the RWP will be greater than the LWP. If the CLP IRI measurements exceed either or both of the LWP and RWP measurements, then the researchers hypothesize that it was caused by something other than normal traffic loadings such as volumetric changes in the subgrade. The imaging system was used to measure and locate cracks in the asphaltic concrete roadway surface, providing insights into the types of distress mechanisms occurring in the pavement structure.

The test sections were assessed on two occasions: June 2017 and June 2018. The service life of the pavements were approximately 18 months (June 2017) and 30 months (June 2018) at the assessment times. Effects of inundation can be measured on the roadway because it had been inundated twice at the June 2017 assessment date and once more by June 2018. DOTD’s International Roughness Index (IRI) specification requires that this type of roadway have an IRI of less than 75 in./mile at the time of construction [51]. Pavement surface cracking was not visible at the time of the first cross-section survey (12-7-2015) according to

LTTRC's cross-section survey crew [52]. Longitudinal surface cracking was the only type of cracking visible at the June 2017 and 2018 assessments. DOTD considers rutting values greater than 0.5 in. to be significant and in need of mitigation. The IRI, rutting, and longitudinal cracking data were calculated and catalogued for each 50-ft. segment within each test site, allowing for statistical comparisons which will be described later.

### **Falling Weight Deflectometer**

Falling weight deflectometer testing was conducted in July 2018 on each test site. Three points were acquired for each test site using a load of approximately 9,000 lb. [53]. The field data was used to obtain the resilient modulus ( $M_r$ ) values for each of the pavement layers using Dynatest's ELMOD 6 backcalculation software. In this report, the  $M_r$  values from the subgrade will be discussed. The in-place structural number ( $SN_{eff}$ ) was calculated using methods in accordance with 1993 AASHTO design guide [12]. The  $SN_{eff}$  was compared to the  $SN_{new}$ , with  $SN_{new}$  referring to the structural number for newly constructed pavement in Louisiana. Layer coefficients of 0.14 SN/in. are typically used by DOTD for newly constructed soil cement and stone base course while 0.44 SN/in. are typically used for newly constructed AC pavement. The base course layer is multiplied by 0.9 to account for drainage [56]. Using the layer coefficients listed above and the thickness values in Table 1, the  $SN_{new}$  for Sites 1 and 3-6 were 2.6 SN while the  $SN_{new}$  for Site 2 was 3.1 SN.

### **Data Analysis and Statistical Testing**

Data from the cross-sections could not be compared using statistical testing; instead, data points were compared to each other within each cross-section as well as compared temporally at each survey date. The difference in elevation from the initial survey (12-7-2015) is what will be discussed in this paper. For example, the measured elevation at the centerline (point 0 on Figure 11) was 30831.74 mm on 12-7-2015 and 30834.18 on 4-25-2016. The difference between the two (30834.18 – 30831.74) equals 2.44 mm. Positive numbers correspond to elevation increases while negative numbers correspond to decreases relative to the initial survey. This method allowed the authors to chart the differential movements across the transverse profile and thus provide evidence of damage to the roadway structure, which will be discussed in detail later.

The statistical test method used to analyze and compare the data from the profiler (IRI, Rutting, Longitudinal cracks) and the FWD ( $M_r$ ,  $SN_{eff}$ ) was the Fisher least square difference test [54-55]. The output from the statistical tests were assigned letters [54-55]. Test sites with similar letters inferred that those sites had similar mean values and vice versa. Minitab 16 was used to conduct the statistical testing.



## DISCUSSION OF RESULTS

### Cross-section Survey

#### Site 1A Cross-section Results

Table 5 and Table 6 and Figures 12 and 13 present the cross-section results. Table 5 provides the elevations (mm) of each cross-section point as well as the dates on which they were taken for informational purposes. Table 6 presents the results of the change in elevation for each cross-section point from the initial preflooded event (12-7-2015). For example, the measured elevation of the center line point (0) on 12-7-2015 was 30831.74 mm and was 30834.18 on 4-25-16, refer to Table 5. The difference between the two (30834.18-30831.74) equals 2.44 mm as presented in Table 6. The same computations were performed for each cross-section point at each date and a similar logic was followed for the remaining cross-section locations in the test sites. For clarity purposes, the first row in Table 6 is for 12/7/2015 with all the values in that row being equal to zero.

This location has the highest elevations of the test sections and is also the only one where trees were not present adjacent to the roadway right-of-way. As such, it provides some interesting information regarding the effects of trees on embankment volumetric changes during flooding events.

First the measured differences in elevation changed between Site 1A (no trees) and Site 1(trees) on 4-25-2016, which was after the first flooding event. The hypothesis that trees create a zone of permanent desiccation as presented in Figure 6 was authenticated by the survey measurements presented in Tables 5 through 8 and Figures 12 through 15. The subgrade soil type in both sections 1A and 1 was a clay with an AASHTO designation of A-7(6), refer to Table 2. However, the increase in elevation at the centerline (0), was 2.44 mm in section 1A and 12.50 mm in section 1 according to the survey measurement on 4-25-16. The probable reason for this difference was that the in-place moisture content at site 1 was lower than the in-place moisture content at Site 1A prior to the inundation event. Therefore, after the inundation event, there was a greater moisture content increase at Site 1 than Site 1A which in turn translates into a greater volume change in the embankment at Site 1 than Site 1A. The differences in the elevation increase (12.50 mm versus 2.44 mm) has far reaching implications in that (1) inundation of roadways where trees are present will be more damaged than roadways without trees, and (2) roadways will be damaged by inundation especially if expansive clays are present due to volume changes. The effects of saturation on

the strength or load carrying capacity of the pavement, base course, and subgrade due to inundation is well documented and will not be expounded upon in this report [7, 8, 11, 56-60].

Further interesting observations from the survey measurements from Site 1A were that some points showed elevation increases while others showed elevation decreases across the roadway cross-section. One plausible explanation is that because of differential movement in the subgrade, semi-rigidity of the soil cement base course, and partial rigidity of the AC layer, an upward movement at one location may cause a downward movement at the adjacent location. A detailed finite element analysis, which is beyond the scope of this report, could validate this. This phenomenon though does fortify the notion that differential movements are occurring at roadway surface and those movements will induce stress into the AC layer which will eventually if not immediately lead to damage. In fact, careful examination of the values in Table 6, Figure 12, and Figure 13 reveal the obvious movements of each point as well as the differences of movement of each point over the course of the cross-section surveys (12-7-2015 to 3-15-18) as well as the effect of inundation.

**Table 5**  
**Cross-section data for Site 1A**

Survey Date	Distance (mm)											Elevations of cross-section points (mm)
	-3048	-2743.2	-2438.4	-2133.6	-1524	0	1706.88	2316.48	2621.28	2926.08	3230.88	
12/7/2015	30764.99	30773.83	30779.62	30786.93	30800.04	30831.74	30790.90	30767.43	30756.76	30745.18	30734.51	
4/25/2016	30763.77	30774.13	30777.48	30784.80	30804.31	30834.18	30790.59	30768.04	30756.45	30746.40	30732.07	
6/16/2016	30760.00	30767.00	30774.00	30781.00	30796.00	30829.00	30786.00	30764.00	30754.00	30742.00	30728.00	
9/20/2016	30759.00	30765.00	30772.00	30779.00	30795.00	30828.00	30786.00	30764.00	30754.00	30743.00	30729.00	
12/6/2016	30755.00	30762.00	30768.00	30774.00	30790.00	30824.00	30781.00	30759.00	30749.00	30738.00	30723.00	
4/25/2017	30757.00	30764.00	30770.00	30776.00	30792.00	30826.00	30783.00	30762.00	30751.00	30740.00	30726.00	
7/13/2017	30757.00	30764.00	30771.00	30777.00	30792.00	30826.00	30783.00	30762.00	30752.00	30740.00	30727.00	
9/15/2017	30764.00	30771.00	30778.00	30785.00	30800.00	30834.00	30789.00	30768.00	30758.00	30746.00	30732.00	
12/6/2017	30759.00	30766.00	30772.00	30779.00	30796.00	30829.00	30785.00	30763.00	30753.00	30742.00	30728.00	
3/15/2018	30762.00	30769.00	30776.00	30783.00	30799.00	30832.00	30789.00	30766.00	30755.00	30744.00	30730.00	

**Table 6**  
**Changes in cross-section elevations from 12/7/2015 for Site 1A**

Survey dates	Distance (mm)											Change in Elevation (mm) From 12/7/2015
	-3048	-2743.2	-2438.4	-2133.6	-1524	0	1706.88	2316.48	2621.28	2926.08	3230.88	
12/7/2015	0.00	0.00	0.00	0.00	0.00	0.00	0.00	0.00	0.00	0.00	0.00	0.00
4/25/2016	-1.22	0.30	-2.13	-2.13	4.27	2.44	-0.30	0.61	-0.30	1.22	-2.44	
6/16/2016	-4.99	-6.83	-5.62	-5.93	-4.04	-2.74	-4.90	-3.43	-2.76	-3.18	-6.51	
9/20/2016	-5.99	-8.83	-7.62	-7.93	-5.04	-3.74	-4.90	-3.43	-2.76	-2.18	-5.51	
12/6/2016	-9.99	-11.83	-11.62	-12.93	-10.04	-7.74	-9.90	-8.43	-7.76	-7.18	-11.51	
4/25/2017	-7.99	-9.83	-9.62	-10.93	-8.04	-5.74	-7.90	-5.43	-5.76	-5.18	-8.51	
7/13/2017	-7.99	-9.83	-8.62	-9.93	-8.04	-5.74	-7.90	-5.43	-4.76	-5.18	-7.51	
9/15/2017	-0.99	-2.83	-1.62	-1.93	-0.04	2.26	-1.90	0.57	1.24	0.82	-2.51	
12/6/2017	-5.99	-7.83	-7.62	-7.93	-4.04	-2.74	-5.90	-4.43	-3.76	-3.18	-6.51	
3/15/2018	-2.99	-4.83	-3.62	-3.93	-1.04	0.26	-1.90	-1.43	-1.76	-1.18	-4.51	

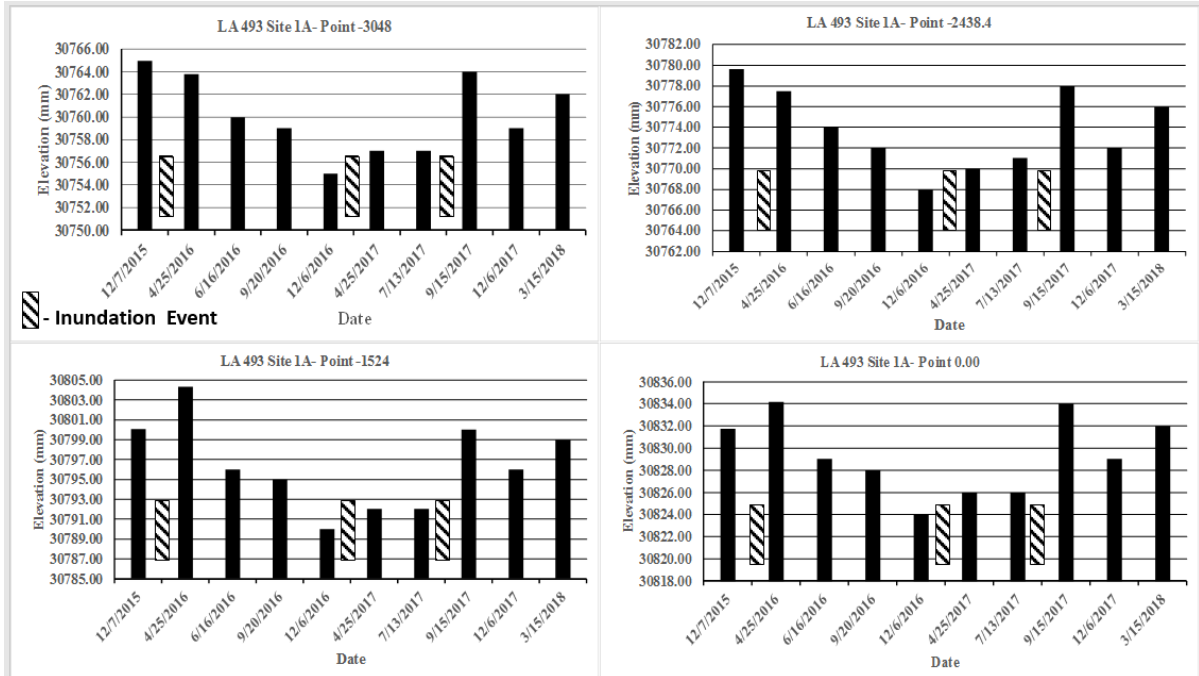


Figure 12  
Charts of cross-section points for Site 1A

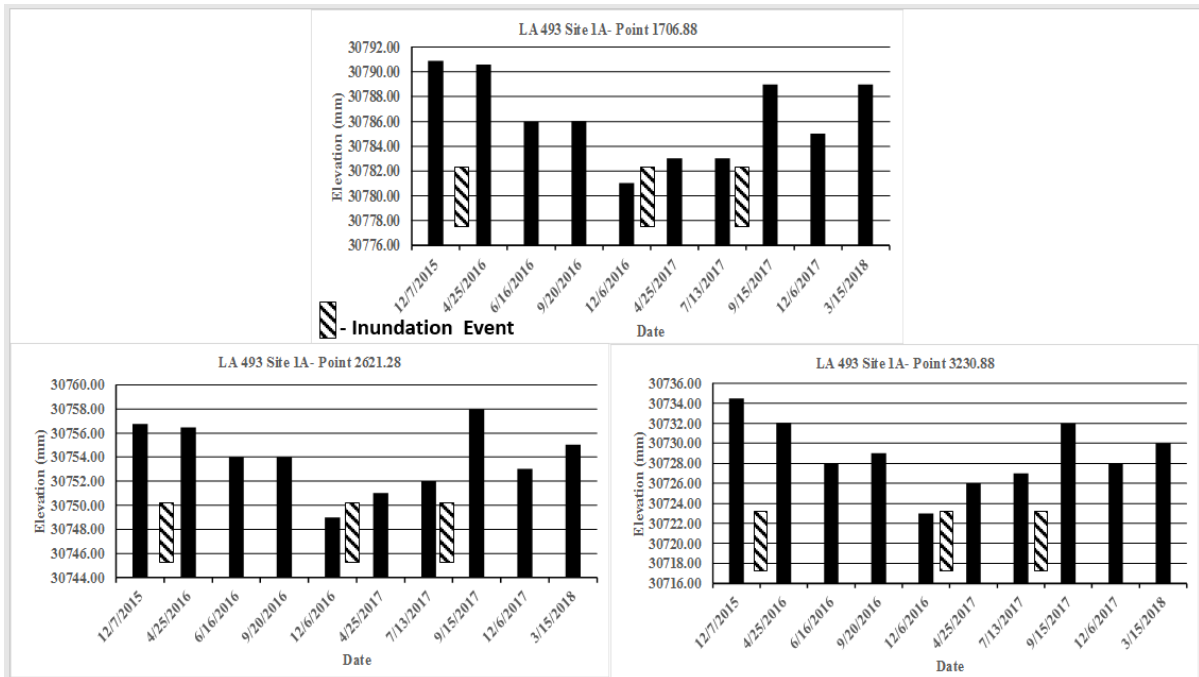


Figure 13  
Charts of cross-section points for Site 1A

### Site 1 Cross-section Results

Table 7 and Table 8 and Figure 14 and Figure 15 present the results for the cross-section surveys. For this cross-section, no data is reported for the point 3230.88 because the edge of the road where this point was originally taken was damaged by heavy machinery. The elevation of the cross-section points (4-25-2016) all increased after the first flooding event with elevation increases ranging from 19.20 mm to 10.97 mm. As with section 1A, no adjacent point increased with a similar magnitude indicating that bending stresses were induced into the AC pavement and underlying layers. The trend toward increasing elevations continued until 12/6/2016 at which time the centerline (0) and left side of the roadway (-distances) reduced in magnitude while there was a general increase in magnitude on the right side (+ distances) of the roadway. The reasons for these differences between the left side and right side of the roadway is unknown. However, the reasons for the decreases in elevation (shrinking) can be explained because no flooding occurred between the 4/25/2016 and 12/6/2016. This trend generally reversed (increasing elevations) in the period between 4/25/2017 and 3/15/2018, which is probably the result of the two flooding events (February 2017 to April 2017) and (July 2017 to August 2017). It should be noted that on 3/15/2018, the AC surface was 59.51 mm higher than the time of the first cross-sectional survey on 12/7/2015 and that no point measured on the cross-section had the same magnitude.

**Table 7**  
**Cross-section data for Site 1**

Survey Dates	Distance (mm)										Elevation of cross-section points (mm)
	-3048	-2743.2	-2438.4	-2133.6	-1524	0	1706.88	2316.48	2621.28	2926.08	
12/7/2015	30078.88	30086.20	30091.08	30095.34	30104.49	30143.81	30111.80	30094.73	30089.86	30082.54	
4/25/2016	30091.38	30100.83	30106.62	30113.94	30123.69	30156.30	30122.77	30110.28	30105.71	30099.61	
6/16/2016	30094.00	30101.00	30106.00	30114.00	30125.00	30157.00	30122.00	30110.00	30105.00	30100.00	
9/20/2016	30094.00	30102.00	30106.00	30114.00	30126.00	30158.00	30122.00	30111.00	30105.00	30099.00	
12/6/2016	30075.00	30084.00	30089.00	30096.00	30109.00	30154.00	30134.00	30123.00	30117.00	30109.00	
4/25/2017	30091.00	30098.00	30104.00	30112.00	30124.00	30156.00	30120.00	30108.00	30102.00	30098.00	
7/13/2017	30099.00	30105.00	30113.00	30126.00	30158.00	30123.00	30110.00	30105.00	30099.00	30094.00	
9/15/2017	30104.00	30109.00	30117.00	30128.00	30164.00	30128.00	30116.00	30110.00	30104.00	30099.00	
12/6/2017	30099.00	30105.00	30113.00	30126.00	30160.00	30124.00	30112.00	30106.00	30100.00	30095.00	
3/15/2018	30104.00	30110.00	30118.00	30130.00	30164.00	30129.00	30117.00	30111.00	30106.00	30100.00	

**Table 8**  
**Changes in cross-section elevations from 12/7/2015 for Site 1**

Survey Date	Distance (mm)										Change in Elevation (mm) from 12/7/2015.	
	-3048	-2743.2	-2438.4	-2133.6	-1524	0	1706.88	2316.48	2621.28	2926.08		
12/7/2015	0.00	0.00	0.00	0.00	0.00	0.00	0.00	0.00	0.00	0.00		0.00
4/25/2016	12.50	14.63	15.54	18.59	19.20	12.50	10.97	15.54	15.85	17.07		17.07
6/16/2016	15.12	14.80	14.92	18.66	20.51	13.19	10.20	15.27	15.14	17.46		17.46
9/20/2016	15.12	15.80	14.93	18.66	21.51	14.20	10.20	16.27	15.14	16.46		16.46
12/6/2016	-3.88	-2.20	-2.07	0.66	4.51	10.20	22.20	28.27	27.14	26.46		26.46
4/25/2017	12.12	11.80	12.93	16.66	19.51	12.20	8.20	13.27	12.14	15.46		15.46
7/13/2017	20.12	18.80	21.93	30.66	53.51	-20.80	-1.80	10.27	9.14	11.46		11.46
9/15/2017	25.12	22.80	25.93	32.66	59.51	-15.80	4.20	15.27	14.14	16.46		16.46
12/6/2017	20.12	18.80	21.93	30.66	55.51	-19.80	0.20	11.27	10.14	12.46		12.46
3/15/2018	25.12	23.80	26.93	34.66	59.51	-14.80	5.20	16.27	16.14	17.46	17.46	

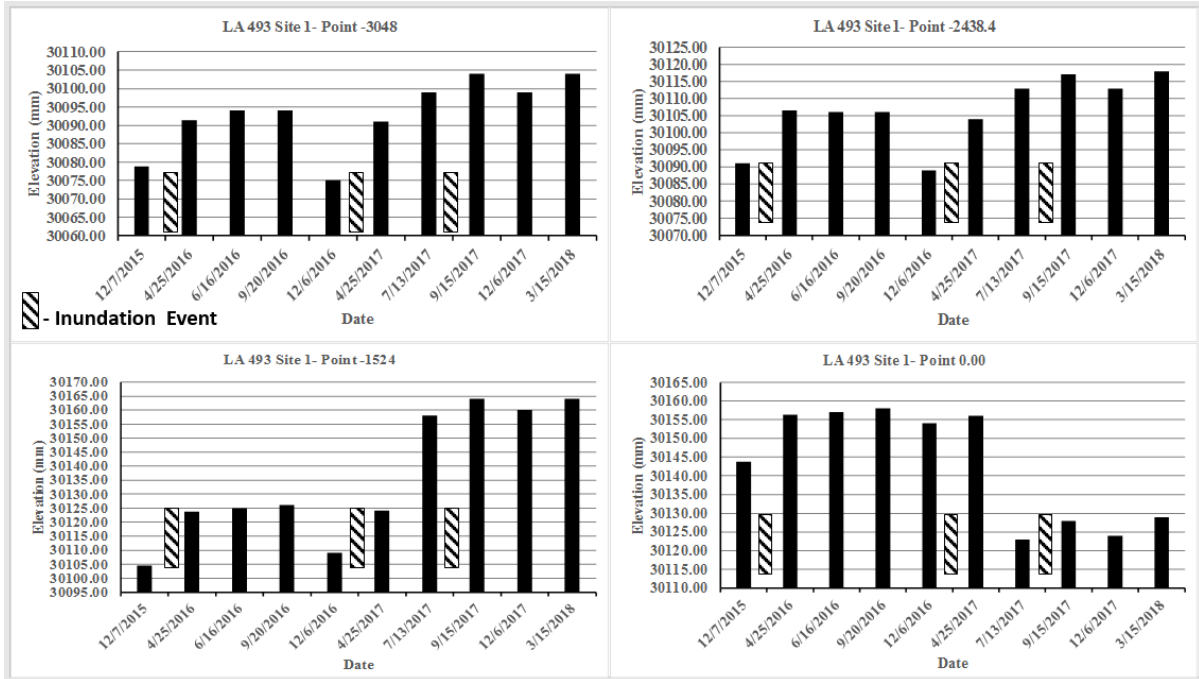


**Figure 14**  
**Charts of cross-section points for Site 1**

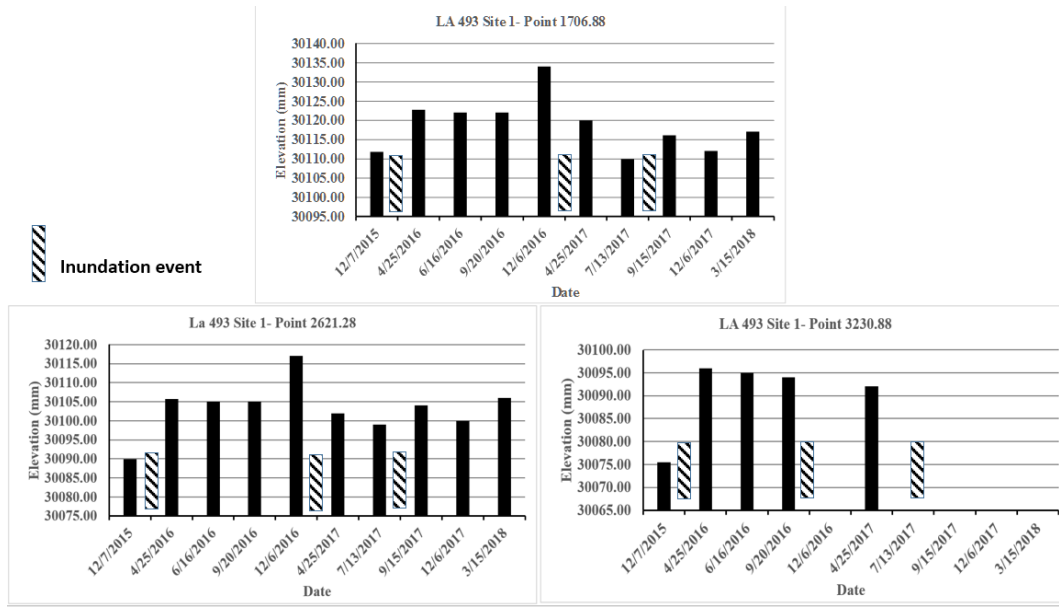


**Figure 15**  
**Charts of cross-section points for Site 1**

### Site 2 Cross-section Results

Table 9 and Table 10 and Figure 16 and Figure 17 present the results for Site 2. As with the previous sites, there was an increase in elevation (17.07 mm) at the centerline on 4/25/2016. The magnitude of elevation increase ranged from 30.78 mm to 10.67 mm with the right side of the roadway having a higher magnitude of increase than the left. No point on the roadway had the same magnitude of increase giving further credence to stresses being induced in the roadway by inundation.

There was a general trend in decreasing elevations from 4/25/2016 to 12/6/2016. From there elevations generally increased at varying rates due to the flooding events in (February 2017 to April 2017) and (July 2017 to August 2017). The elevation at the centerline (0) was 29.06 mm higher than it was on 12/7/2015. The elevation increases on the left side of the roadway were less than on the right side of the roadway with the elevation increase being as high as 45.07 mm. This trend was opposite at Site 1. What this does point to, however, is that volumetric changes in the embankment were highly variable.

**Table 9**  
**Cross-section data for Site 2**

Survey Date	Distance (mm)											Elevations of cross-section points (mm)
	-3048.00	-2743.20	-2438.40	-2133.60	-1524.00	0.00	1706.88	2316.48	2621.28	2926.08	3230.88	
12/7/2015	30144.72	30150.51	30151.73	30158.44	30168.80	30202.94	30173.98	30160.87	30153.25	30146.24	30138.93	
4/25/2016	30155.39	30165.14	30169.71	30173.68	30184.04	30220.01	30193.79	30179.16	30177.94	30174.29	30169.71	
6/16/2016	30161.00	30168.00	30173.00	30177.00	30189.00	30224.00	30201.00	30190.00	30185.00	30182.00	30178.00	
9/20/2016	30157.00	30165.00	30169.00	30174.00	30186.00	30222.00	30199.00	30185.00	30179.00	30175.00	30170.00	
12/6/2016	30156.00	30164.00	30168.00	30173.00	30185.00	30221.00	30198.00	30183.00	30176.00	30171.00	30163.00	
4/25/2017	30157.00	30164.00	30169.00	30173.00	30184.00	30222.00	30200.00	30187.00	30181.00	30178.00	30173.00	
7/13/2017	30158.00	30166.00	30170.00	30175.00	30188.00	30225.00	30203.00	30189.00	30183.00	30179.00	30174.00	
9/15/2017	30162.00	30170.00	30174.00	30179.00	30192.00	30229.00	30206.00	30192.00	30185.00	30182.00	30176.00	
12/6/2017	30158.00	30166.00	30170.00	30175.00	30188.00	30226.00	30204.00	30189.00	30183.00	30179.00	30173.00	
3/15/2018	30164.00	30172.00	30176.00	30181.00	30194.00	30232.00	30212.00	30198.00	30192.00	30189.00	30184.00	

**Table 10**  
**Changes in cross-section elevations from 12/7/2015 for Site 2**

Survey Dates	Distances (mm)											Change in Elevation (mm) from 12/7/2015
	-3048	-2743.2	-2438.4	-2133.6	-1524	0	1706.88	2316.48	2621.28	2926.08	3230.88	
12/7/2015	0.00	0.00	0.00	0.00	0.00	0.00	0.00	0.00	0.00	0.00	0.00	
4/25/2016	10.67	14.63	17.98	15.24	15.24	17.07	19.81	18.29	24.69	28.04	30.78	
6/16/2016	16.28	17.49	21.27	18.56	20.20	21.06	27.02	29.13	31.75	35.76	39.07	
9/20/2016	12.28	14.49	17.27	15.56	17.20	19.06	25.02	24.13	25.75	28.76	31.07	
12/6/2016	11.28	13.49	16.27	14.56	16.20	18.06	24.02	22.13	22.75	24.76	24.07	
4/25/2017	12.28	13.49	17.27	14.56	15.20	19.06	26.02	26.13	27.75	31.76	34.07	
7/13/2017	13.28	15.49	18.27	16.56	19.20	22.06	29.02	28.13	29.75	32.76	35.07	
9/15/2017	17.28	19.49	22.27	20.56	23.20	26.06	32.02	31.13	31.75	35.76	37.07	
12/6/2017	13.28	15.49	18.27	16.56	19.20	23.06	30.02	28.13	29.75	32.76	34.07	
3/15/2018	19.28	21.49	24.27	22.56	25.20	29.06	38.02	37.13	38.75	42.76	45.07	

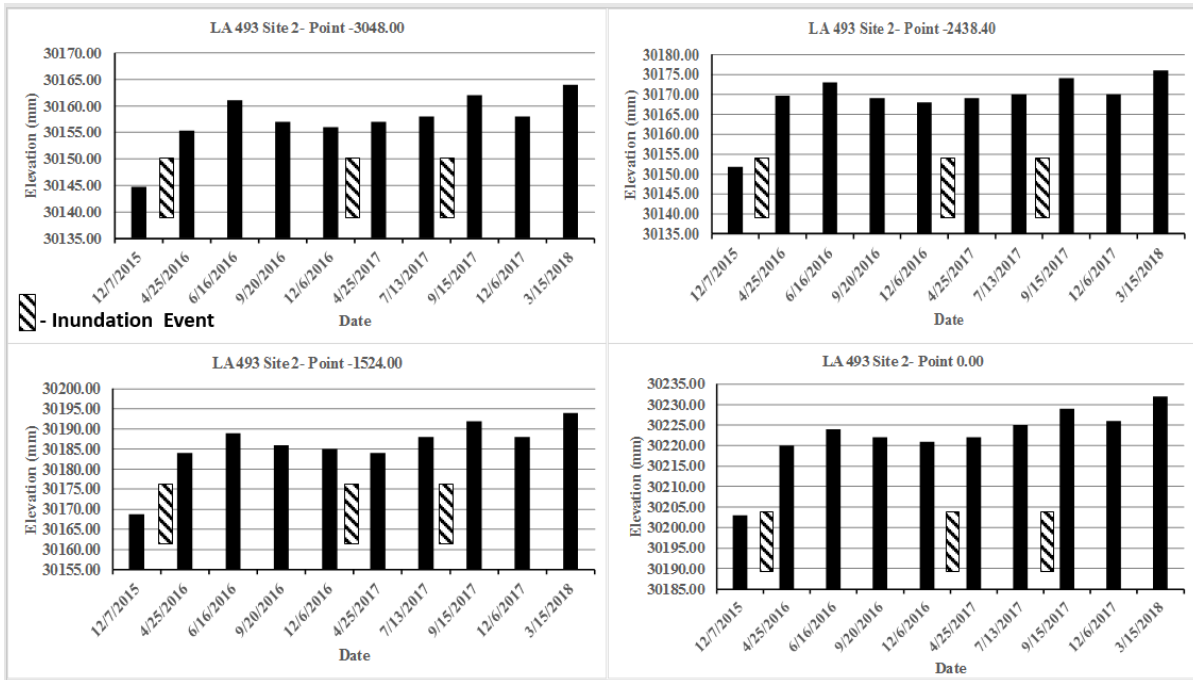


**Figure 16**  
**Charts of cross-sections for Site 2**

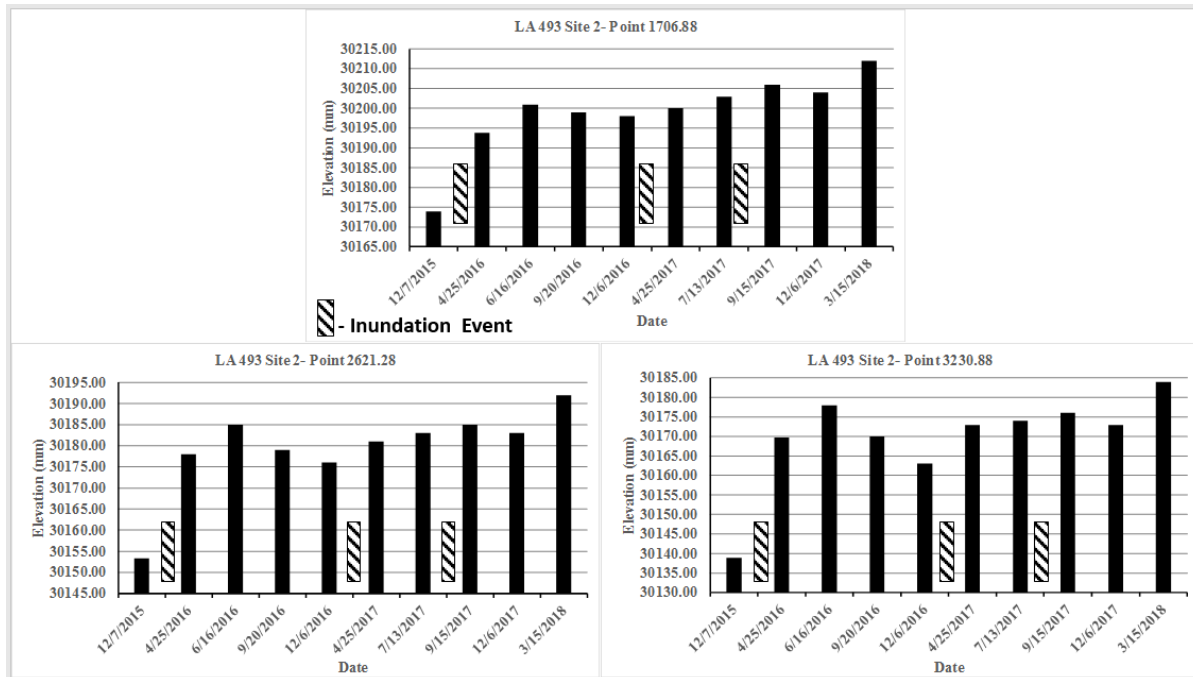


**Figure 17**  
**Charts of cross-sections elevations from 12/7/2015 for Site 2**

### Site 3 Cross-section Results

Table 11 and Table 12 and Figure 18 and Figure 19 present the results for Site 3. As with the previous sites, there was an increase in elevation at the centerline on 4/25/2016 and its magnitude was 37.80 mm. The magnitude of elevation increase ranged from 44.20 mm to 24.38 mm with the left side of the roadway having a higher magnitude of increase than the right. The points on the roadway had differing magnitudes of elevation increases.

There was a general trend of continual elevation increases on the left side of the roadway and elevation decreases on the right side of the roadway up to 12/6/2016. Elevation increases in general were measured for the remainder of the cross-sectional surveys. The maximum elevation increase was 63.47 mm with the minimum increase being 46.51 mm. The right side of the roadway had higher elevation increase magnitudes than the left side; once again demonstrating the high variability of volumetric changes.

**Table 11**  
**Cross-section data for Site 3**

Survey Dates	Distance (mm)											Elevations of cross-section points (mm)
	-3048.00	-2743.20	-2438.40	-2133.60	-1524.00	0.00	1706.88	2316.48	2621.28	2926.08	3230.88	
12/7/2015	30025.85	30035.60	30041.70	30047.49	30059.07	30110.28	30107.53	30107.53	30107.23	30105.40	30104.18	
4/25/2016	30059.99	30069.13	30076.44	30091.68		30148.07	30144.42	30137.40	30132.83	30130.70	30128.57	
6/16/2016	30056.00	30064.00	30071.00	30078.00	30094.00	30152.00	30150.00	30137.00	30134.00	30133.00	30127.00	
9/20/2016	30059.00	30069.00	30073.00	30080.00	30096.00	30157.00	30156.00	30146.00	30140.00	30136.00	30129.00	
12/6/2016	30077.00	30084.00	30090.00	30097.00	30111.00	30155.00	30136.00	30123.00	30119.00	30112.00	30107.00	
4/25/2017	30069.00	30079.00	30078.00	30085.00	30100.00	30160.00	30161.00	30150.00	30148.00	30143.00	30138.00	
7/13/2017	30073.00	30077.00	30083.00	30089.00	30103.00	30162.00	30164.00	30156.00	30154.00	30150.00	30145.00	
9/15/2017	30077.00	30080.00	30086.00	30091.00	30105.00	30165.00	30168.00	30161.00	30162.00	30158.00	30154.00	
12/6/2017	30073.00	30084.00	30084.00	30089.00	30102.00	30162.00	30165.00	30160.00	30159.00	30161.00	30155.00	
3/15/2018	30079.00	30084.00	30089.00	30094.00	30108.00	30167.00	30171.00	30168.00	30169.00	30168.00	30165.00	

**Table 12**  
**Changes in cross-section elevations from 12/7/2015 for Site 3**

Survey Dates	Distances (mm)											Change in Elevation (mm) from 12/7/2015
	-3048	-2743.2	-2438.4	-2133.6	-1524	0	1706.88	2316.48	2621.28	2926.08	3230.88	
12/7/2015	0.00	0.00	0.00	0.00	0.00	0.00	0.00	0.00	0.00	0.00	0.00	
4/25/2016	34.14	33.53	34.75	44.20		37.80	36.88	29.87	25.60	25.30	24.38	
6/16/2016	30.15	28.40	29.30	30.51	34.93	41.72	42.47	29.47	26.77	27.60	22.82	
9/20/2016	33.15	33.40	31.30	32.51	36.93	46.72	48.47	38.47	32.77	30.60	24.82	
12/6/2016	51.15	48.40	48.30	49.51	51.93	44.72	28.47	15.47	11.77	6.60	2.82	
4/25/2017	43.15	43.40	36.30	37.51	40.93	49.72	53.47	42.47	40.77	37.60	33.82	
7/13/2017	47.15	41.40	41.30	41.51	43.93	51.72	56.47	48.47	46.77	44.60	40.82	
9/15/2017	51.15	44.40	44.30	43.51	45.93	54.72	60.47	53.47	54.77	52.60	49.82	
12/6/2017	47.15	48.40	42.30	41.51	42.93	51.72	57.47	52.47	51.77	55.60	50.82	
3/15/2018	53.15	48.40	47.30	46.51	48.93	56.72	63.47	60.47	61.77	62.60	60.82	

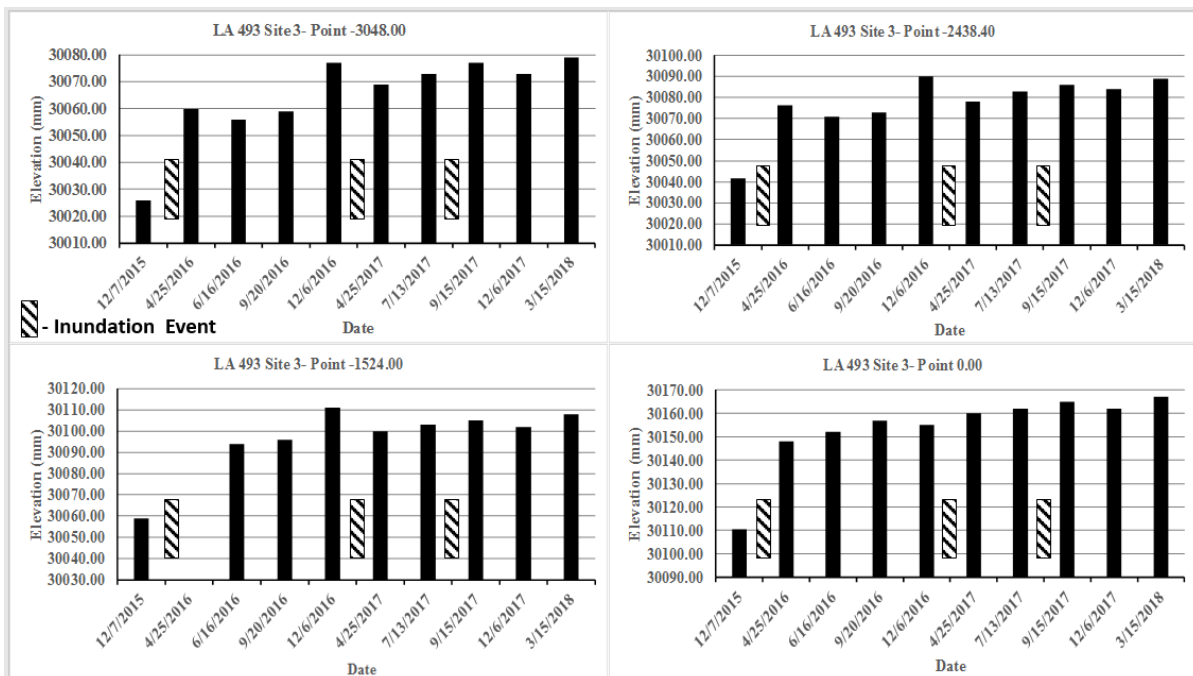


**Figure 18**  
**Charts of cross-section points for Site 3**

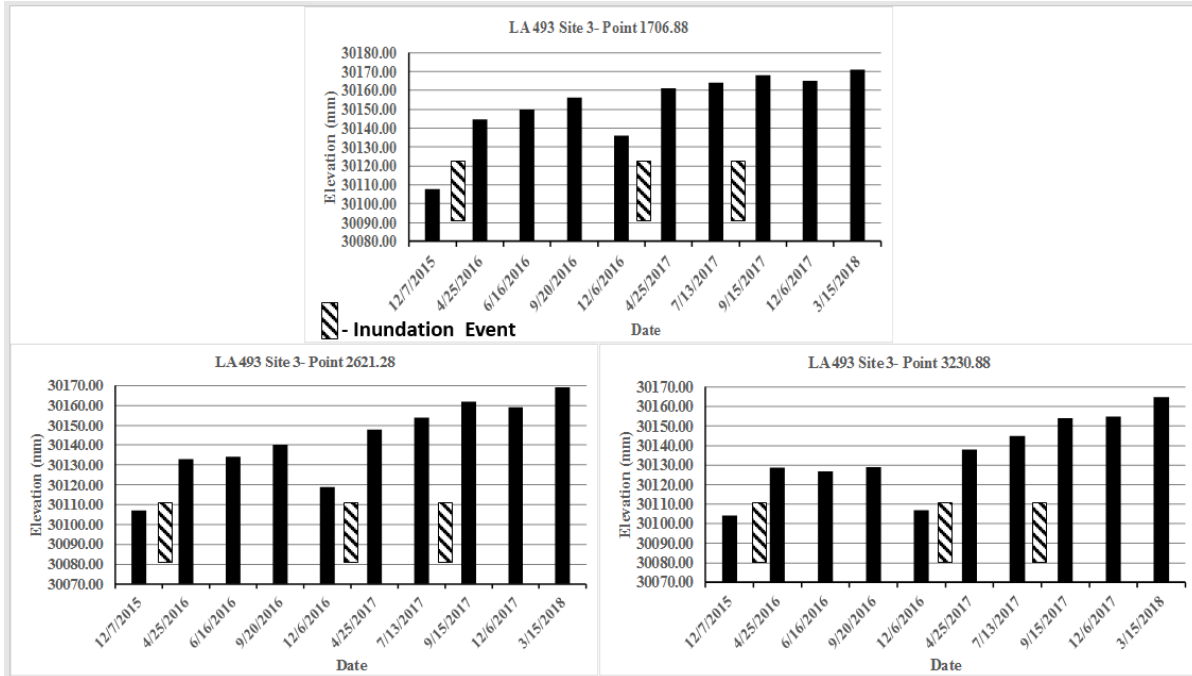


**Figure 19**  
**Charts of cross-section points for Site 3**

**Site 4 Cross-section Results**

Table 13 and Table 14 and Figure 20 and Figure 21 present the results for Site 4. As with the previous sites, there was an increase in elevation at the centerline on 4/25/2016 and its magnitude was 44.50 mm. The magnitude of elevation increase ranged from 44.5 mm to 31.09 mm with the right side of the roadway having a higher magnitude of increase than the left. The points on the roadway had differing magnitudes of elevation increases.

Unlike the previous sites, the cross-sections maintained a fairly consistent elevation from 4/25/2016 to 12/6/2016. From there a consistent increase in elevation for the cross-section was measured. At 3/15/2018 the maximum elevation increase was 55.42 mm with the right side of the roadway having higher elevation increases than the left.

**Table 13**  
**Cross-section data for Site 4**

Survey dates	Distance (mm)										
	-3048.00	-2743.20	-2438.40	-2133.60	-1524.00	0.00	1706.88	2316.48	2621.28	2926.08	3230.88
12/7/2015	30262.07	30266.03	30272.13	30278.83	30289.50	30326.08	30288.59	30277.31	30270.91	30262.68	30255.97
4/25/2016	30293.16	30299.56	30307.18	30313.88	30330.04	30370.58	30329.12	30315.10	30307.18	30298.95	30290.41
6/16/2016	30297.00	30302.00	30310.00	30317.00	30332.00	30372.00	30332.00	30319.00	30310.00	30302.00	30294.00
9/20/2016	30298.00	30303.00	30311.00	30317.00	30331.00	30371.00	30331.00	30317.00	30308.00	30301.00	30294.00
12/6/2016	30300.00	30305.00	30312.00	30318.00	30333.00	30372.00	30331.00	30317.00	30307.00	30299.00	30290.00
4/25/2017	30304.00	30310.00	30317.00	30322.00	30336.00	30374.00	30335.00	30323.00	30314.00	30307.00	30298.00
7/13/2017	30305.00	30310.00	30318.00	30323.00	30336.00	30375.00	30337.00	30324.00	30316.00	30309.00	30301.00
9/15/2017	30308.00	30313.00	30320.00	30326.00	30339.00	30377.00	30339.00	30326.00	30319.00	30311.00	30302.00
12/6/2017	30307.00	30312.00	30318.00	30324.00	30337.00	30375.00	30337.00	30324.00	30316.00	30308.00	30299.00
3/15/2018	30312.00	30317.00	30323.00	30328.00	30341.00	30380.00	30344.00	30331.00	30325.00	30318.00	30310.00

Elevations of cross-section points (mm)

**Table 14**  
**Changes in cross-section elevations from 12/7/2015 for Site 4**

Survey Dates	Distance (mm)										
	-3048	-2743.2	-2438.4	-2133.6	-1524	0	1706.88	2316.48	2621.28	2926.08	3230.88
12/7/2015	0.00	0.00	0.00	0.00	0.00	0.00	0.00	0.00	0.00	0.00	0.00
4/25/2016	31.09	33.53	35.05	35.05	40.54	44.50	40.54	37.80	36.27	36.27	34.44
6/16/2016	34.93	35.97	37.87	38.17	42.50	45.92	43.41	41.69	39.09	39.32	38.03
9/20/2016	35.93	36.97	38.87	38.17	41.50	44.92	42.42	39.69	37.09	38.32	38.03
12/6/2016	37.93	38.97	39.87	39.17	43.50	45.92	42.42	39.69	36.09	36.32	34.03
4/25/2017	41.93	43.97	44.87	43.17	46.50	47.92	46.42	45.69	43.09	44.32	42.03
7/13/2017	42.93	43.97	45.87	44.17	46.50	48.92	48.42	46.69	45.09	46.32	45.03
9/15/2017	45.93	46.97	47.87	47.17	49.50	50.92	50.42	48.69	48.09	48.32	46.03
12/6/2017	44.93	45.97	45.87	45.17	47.50	48.92	48.42	46.69	45.09	45.32	43.03
3/15/2018	49.93	50.97	50.87	49.17	51.50	53.92	55.42	53.69	54.09	55.32	54.03

Change in Elevation (mm) from 12/7/2015

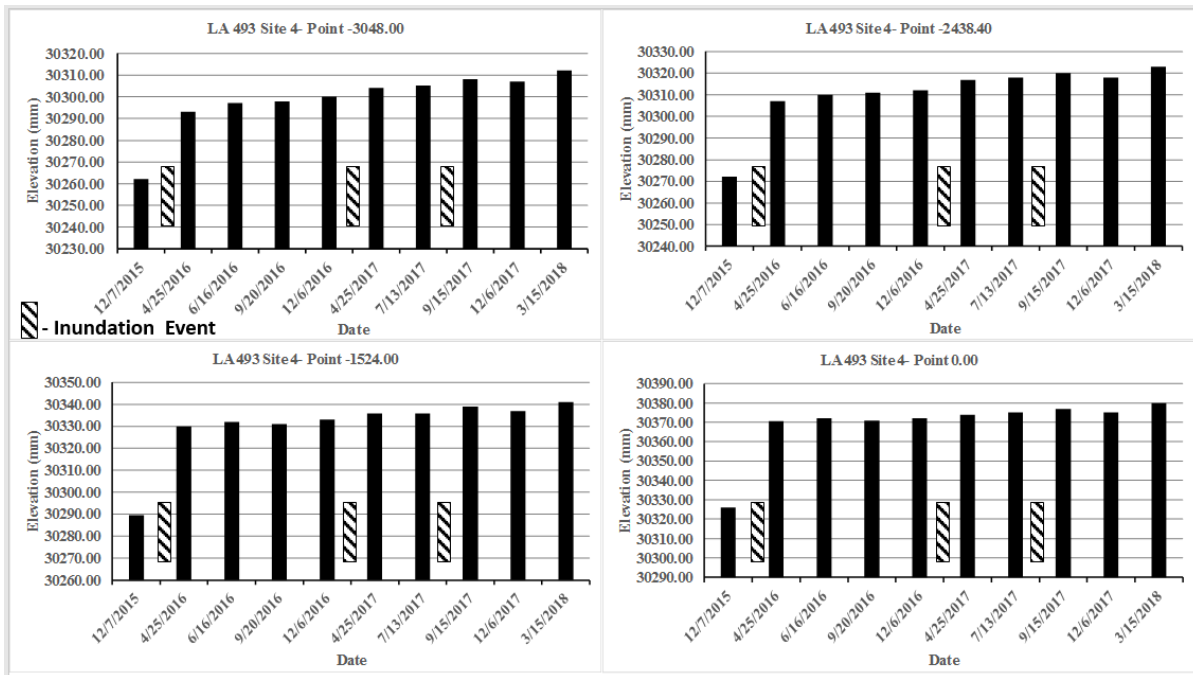


**Figure 20**  
**Charts of cross-section points for Site 4**

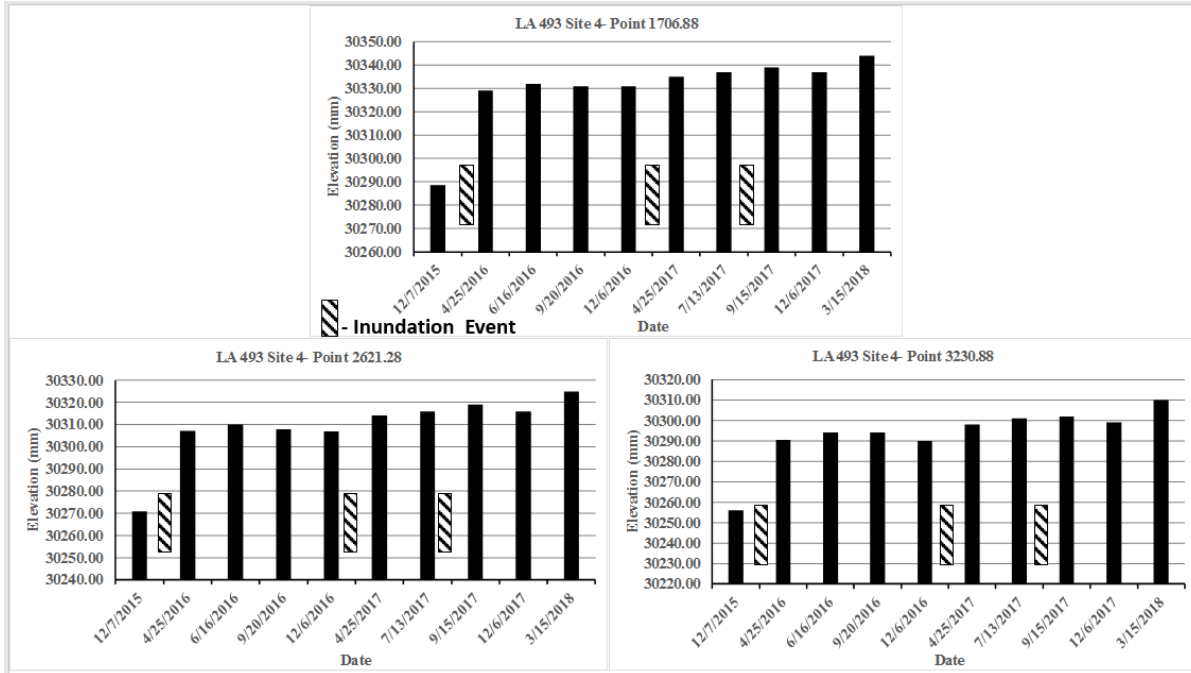


**Figure 21**  
**Charts of cross-section points for Site 4**

**Site 5 Cross-section Results**

Table 15 and Table 16 and Figure 22, and Figure 23 present the results for Site 5. As with the previous sites, there was an increase in elevation at the centerline on 4/25/2016 and its magnitude was 34.44 mm. The magnitude of elevation increase ranged from 34.44 mm to 23.47 mm with the right side of the roadway having a higher magnitude of increase than the left. The points on the roadway had differing magnitudes of elevation increases.

Similar to Site 4, and unlike the previous sites, the cross-sections maintained a fairly consistent elevation from 4/25/2016 to 12/6/2016. From there, a generally consistent increase in elevation for the cross-section was measured. At 3/15/2018, the maximum elevation increase was 45.01 mm with the right side of the roadway having higher elevation increases than the left.

**Table 15**  
**Cross-section data for Site 5**

Survey date	Distance (mm)											Elevations of cross-section points (mm)
	-3048.00	-2743.20	-2438.40	-2133.60	-1524.00	0.00	1706.88	2316.48	2621.28	2926.08	3230.88	
12/7/2015	30121.25	30124.30	30128.57	30133.14	30142.28	30180.99	30148.07	30132.53	30125.21	30120.64	30115.15	
4/25/2016	30145.33	30147.77	30153.25	30159.66	30172.76	30215.43	30175.50	30159.66	30152.95	30146.24	30141.37	
6/16/2016	30147.00	30149.00	30155.00	30161.00	30174.00	30216.00	30178.00	30162.00	30155.00	30149.00	30144.00	
9/20/2016	30147.00	30149.00	30154.00	30160.00	30173.00	30214.00	30177.00	30162.00	30155.00	30149.00	30144.00	
12/6/2016	30149.00	30151.00	30155.00	30162.00	30175.00	30216.00	30179.00	30163.00	30157.00	30150.00	30144.00	
4/25/2017	30151.00	30153.00	30158.00	30164.00	30177.00	30218.00	30181.00	30166.00	30160.00	30154.00	30149.00	
7/13/2017	30154.00	30156.00	30161.00	30166.00	30179.00	30220.00	30184.00	30169.00	30163.00	30157.00	30151.00	
9/15/2017	30155.00	30158.00	30161.00	30168.00	30178.00	30222.00	30186.00	30171.00	30164.00	30159.00	30154.00	
12/6/2017	30152.00	30153.00	30158.00	30164.00	30178.00	30218.00	30183.00	30168.00	30161.00	30156.00	30151.00	
3/15/2018	30160.00	30162.00	30166.00	30171.00	30185.00	30226.00	30192.00	30177.00	30171.00	30165.00	30160.00	

**Table 16**  
**Changes in cross-section elevations from 12/7/2015 for Site 5**

Survey Date	Distance (mm)											Change in Elevation (mm) from 12/7/2015
	-3048	-2743.2	-2438.4	-2133.6	-1524	0	1706.88	2316.48	2621.28	2926.08	3230.88	
12/7/2015	0.00	0.00	0.00	0.00	0.00	0.00	0.00	0.00	0.00	0.00	0.00	
4/25/2016	24.08	23.47	24.69	26.52	30.48	34.44	27.43	27.13	27.74	25.60	26.21	
6/16/2016	25.75	24.70	26.43	27.86	31.72	35.01	29.93	29.47	29.79	28.36	28.85	
9/20/2016	25.75	24.70	25.44	26.86	30.72	33.01	28.93	29.47	29.79	28.36	28.85	
12/6/2016	27.75	26.70	26.44	28.86	32.72	35.01	30.93	30.47	31.79	29.36	28.85	
4/25/2017	29.75	28.70	29.44	30.86	34.72	37.01	32.93	33.47	34.79	33.36	33.85	
7/13/2017	32.75	31.70	32.44	32.86	36.72	39.01	35.93	36.47	37.79	36.36	35.85	
9/15/2017	33.75	33.70	32.44	34.86	35.72	41.01	37.93	38.47	38.79	38.36	38.85	
12/6/2017	30.75	28.70	29.44	30.86	35.72	37.01	34.93	35.47	35.79	35.36	35.85	
3/15/2018	38.75	37.70	37.44	37.86	42.72	45.01	43.93	44.47	45.79	44.36	44.85	

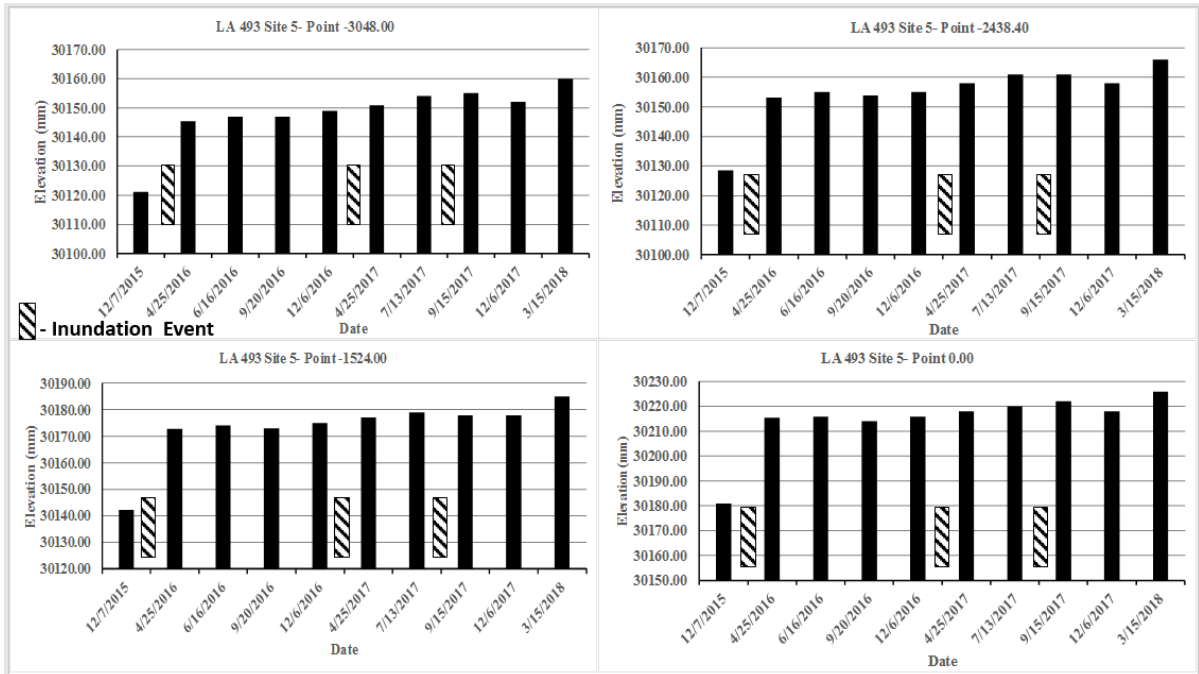


**Figure 22**  
**Charts of cross-section points for Site 5**

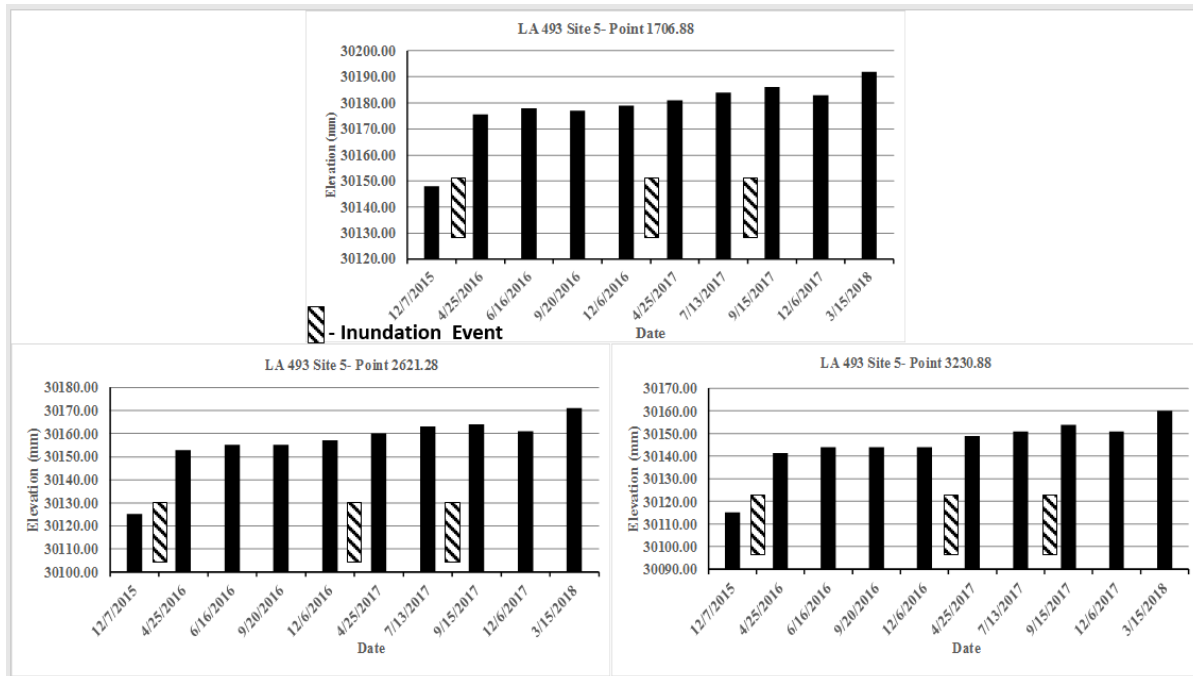


**Figure 23**  
**Charts of cross-section points for Site 5**

### Site 6 Cross-section Results

Table 17 and Table 18 and Figure 24, and Figure 25 present the results for Site 6. As with the previous sites, there was an increase in elevation at the centerline on 4/25/2016 with a magnitude was 18.59 mm. The magnitude of elevation increase ranged from 23.47 mm to 16.15 mm with the left side of the roadway having a higher magnitude increase than the right. The points on the roadway had differing magnitudes of elevation increases.

The cross-sections maintained a fairly consistent elevation from 4/25/2016 to 12/6/2016. From there a general consistent increase in elevation for the cross-section was measured. At 3/15/2018 the maximum elevation increase was 47.46 mm with the left side of the roadway having higher elevation increases than the right.

**Table 17**  
**Cross-section data for Site 6**

Survey dates	Distance (mm)											Elevations of cross-section points (mm)
	-3048.00	-2743.20	-2438.40	-2133.60	-1524.00	0.00	1706.88	2316.48	2621.28	2926.08	3230.88	
12/7/2015	30317.54	30323.33	30329.12	30334.31	30344.36	30385.82	30357.17	30342.84	30333.70	30330.04	30323.33	
4/25/2016	30341.01	30346.19	30350.46	30355.34	30363.87	30404.41	30377.28	30362.04	30354.73	30350.46	30339.49	
6/16/2016	30345.00	30349.00	30353.00	30358.00	30366.00	30407.00	30380.00	30365.00	30358.00	30352.00	30346.00	
9/20/2016	30347.00	30351.00	30353.00	30357.00	30365.00	30407.00	30376.00	30365.00	30360.00	30354.00	30347.00	
12/6/2016	30349.00	30353.00	30356.00	30360.00	30368.00	30409.00	30380.00	30368.00	30363.00	30355.00	30346.00	
4/25/2017	30355.00	30359.00	30361.00	30365.00	30373.00	30414.00	30387.00	30375.00	30370.00	30364.00	30357.00	
7/13/2017	30356.00	30360.00	30362.00	30366.00	30373.00	30415.00	30388.00	30376.00	30371.00	30366.00	30358.00	
9/15/2017	30360.00	30363.00	30365.00	30368.00	30376.00	30417.00	30390.00	30380.00	30375.00	30369.00	30360.00	
12/6/2017	30359.00	30362.00	30364.00	30367.00	30375.00	30416.00	30390.00	30379.00	30374.00	30366.00	30356.00	
3/15/2018	30365.00	30368.00	30368.00	30372.00	30379.00	30420.00	30394.00	30383.00	30379.00	30374.00	30366.00	

**Table 18**  
**Changes in cross-section elevations from 12/7/2015 for Site 6**

Survey Date	Distance (mm)											Change in Elevation (mm) from 12/7/2015
	-3048	-2743.2	-2438.4	-2133.6	-1524	0	1706.88	2316.48	2621.28	2926.08	3230.88	
12/7/2015	0.00	0.00	0.00	0.00	0.00	0.00	0.00	0.00	0.00	0.00	0.00	
4/25/2016	23.47	22.86	21.34	21.03	19.51	18.59	20.12	19.20	21.03	20.42	16.15	
6/16/2016	27.46	25.67	23.88	23.69	21.64	21.18	22.83	22.16	24.30	21.96	22.67	
9/20/2016	29.46	27.67	23.88	22.70	20.64	21.18	18.84	22.16	26.30	23.96	23.67	
12/6/2016	31.46	29.67	26.88	25.70	23.64	23.18	22.84	25.16	29.30	24.96	22.67	
4/25/2017	37.46	35.67	31.88	30.70	28.64	28.18	29.84	32.16	36.30	33.96	33.67	
7/13/2017	38.46	36.67	32.88	31.70	28.64	29.18	30.84	33.16	37.30	35.96	34.67	
9/15/2017	42.46	39.67	35.88	33.70	31.64	31.18	32.84	37.16	41.30	38.96	36.67	
12/6/2017	41.46	38.67	34.88	32.70	30.64	30.18	32.84	36.16	40.30	35.96	32.67	
3/15/2018	47.46	44.67	38.88	37.70	34.64	34.18	36.84	40.16	45.30	43.96	42.67	

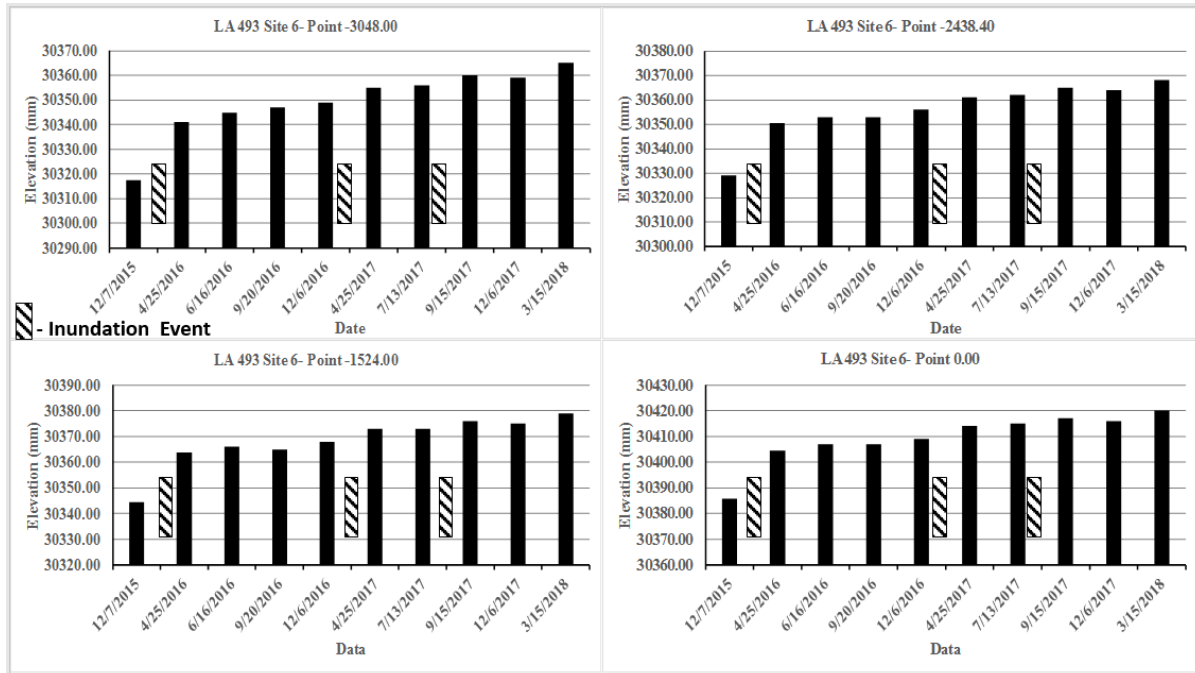


**Figure 24**  
**Charts of cross-section points for Site 6**

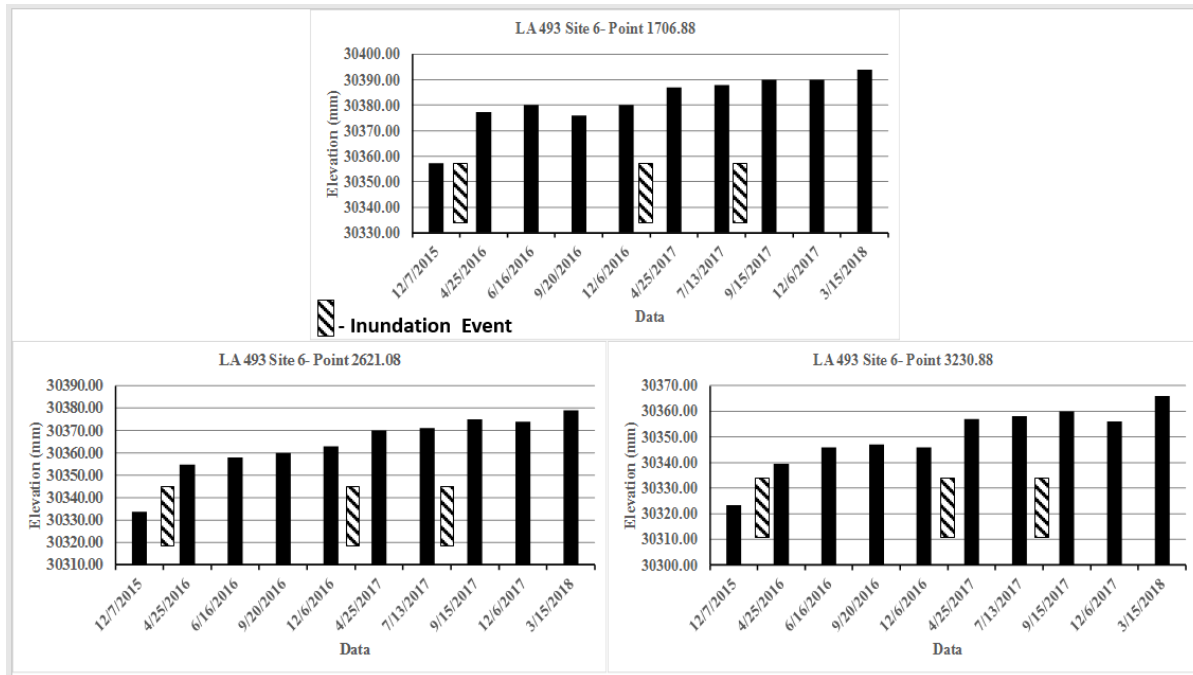


**Figure 25**  
**Charts of cross-section points for Site 6**

### Roadway Profiling and Imaging

#### IRI

There were 42 possible variables per assessment for the IRI data acquired on this project [54-55]. The statistical analysis from the June 2017 assessment yielded 216 possible pairwise combinations, which is excessive, indicating that there is a high degree of variance in the data as presented in Table 19. Figure 26 presents the IRI values for the EB and WB lanes from the June 2017 assessment. The graphs illustrate the high degree of variation in the data. The IRI values for all sites exceeded 75 in./mile on the June 2017 collection date implying that the roadway was rougher than it should be for the amount of time that it has been in service.

Statistical pairwise comparisons from the June 2018 assessment are presented in Table 20 and the data is presented graphically in Figure 27. According to the statistical analysis, the means could be placed into 11 distinct groups. Had there been consistent movements throughout the roadway sections, then the mean values would have been similar. As with the June 2017 assessment, all sites had IRI values exceeding 75 in./mile.

**Table 19**  
**EB and WB descriptive statistical IRI data for the June 2017 assessment**

Variable (2017)	N	Mean (in./mile)	StDev (in./mile)	COV %	Minimum (in./mile)	Maximum (in./mile)	Range (in./mile)
1A_LWP_EB	4	139.8	66.9	47.9	68.1	207.0	138.9
1A_CLP_EB	4	122.8	75.9	61.8	59.9	232.6	172.7
1A_RWP_EB	4	159.2	77.9	48.9	64.7	248.2	183.5
1_LWP_EB	12	121.5	29.9	24.6	66.6	164.0	97.5
1_CLP_EB	12	116.1	27.4	23.6	73.7	171.6	97.9
1_RWP_EB	12	118.2	37.3	31.6	56.7	182.2	125.5
2_LWP_EB	14	87.4	40.0	45.7	41.6	169.3	127.8
2_CLP_EB	14	97.8	43.0	44.0	50.6	170.8	120.2
2_RWP_EB	14	115.6	37.6	32.5	64.4	177.8	113.4
3_LWP_EB	14	86.1	30.4	35.3	51.8	151.1	99.3
3_CLP_EB	14	98.4	32.2	32.8	46.5	161.7	115.2
3_RWP_EB	14	122.4	40.6	33.2	66.1	203.0	136.9
4_LWP_EB	16	131.6	95.8	72.9	49.4	455.0	405.6
4_CLP_EB	16	130.9	79.3	60.6	66.2	393.1	326.9
4_RWP_EB	16	131.4	68.7	52.3	53.6	327.8	274.3
5_LWP_EB	16	105.6	27.7	26.2	46.1	156.1	110.0
5_CLP_EB	16	100.4	24.4	24.3	55.5	133.2	77.7
5_RWP_EB	16	93.9	29.9	31.8	50.9	139.0	88.1
6_LWP_EB	16	85.4	26.2	30.7	44.0	146.4	102.5
6_CLP_EB	16	83.9	27.2	32.4	39.9	133.6	93.7
6_RWP_EB	16	87.3	26.7	30.6	32.5	132.0	99.5
1A_LWP_WB	4	133.1	118.0	88.7	70.9	310.0	239.2
1A_CLP_WB	4	129.3	106.8	82.6	54.6	287.2	232.6
1A_RWP_WB	4	153.7	111.6	72.6	69.7	318.1	248.5
1_LWP_WB	12	114.6	47.0	41.1	43.2	186.0	142.8
1_CLP_WB	12	111.7	47.7	42.7	54.0	216.5	162.5
1_RWP_WB	12	141.4	52.9	37.4	72.6	233.2	160.6
2_LWP_WB	14	92.5	35.8	38.7	49.4	153.8	104.4
2_CLP_WB	14	104.5	49.6	47.5	55.3	204.5	149.2
2_RWP_WB	14	113.3	58.4	51.5	57.0	240.4	183.4
3_LWP_WB	14	85.2	33.8	39.6	51.4	163.7	112.3
3_CLP_WB	14	108.7	49.1	45.2	61.2	226.4	165.2
3_RWP_WB	14	125.6	67.1	53.4	67.5	291.4	223.8
4_LWP_WB	16	121.4	62.0	51.1	59.7	336.4	276.7
4_CLP_WB	16	127.6	81.7	64.0	60.8	414.5	353.6
4_RWP_WB	16	136.8	96.6	70.6	54.0	463.8	409.8
5_LWP_WB	16	111.8	30.6	27.3	65.1	159.3	94.1
5_CLP_WB	16	106.7	28.4	26.6	56.0	154.9	98.9
5_RWP_WB	16	115.2	44.0	38.2	52.3	205.8	153.5
6_LWP_WB	16	96.3	27.3	28.4	65.7	148.6	82.8
6_CLP_WB	16	100.5	31.2	31.0	61.1	166.4	105.3
6_RWP_WB	16	102.3	35.6	34.8	51.9	176.6	124.7

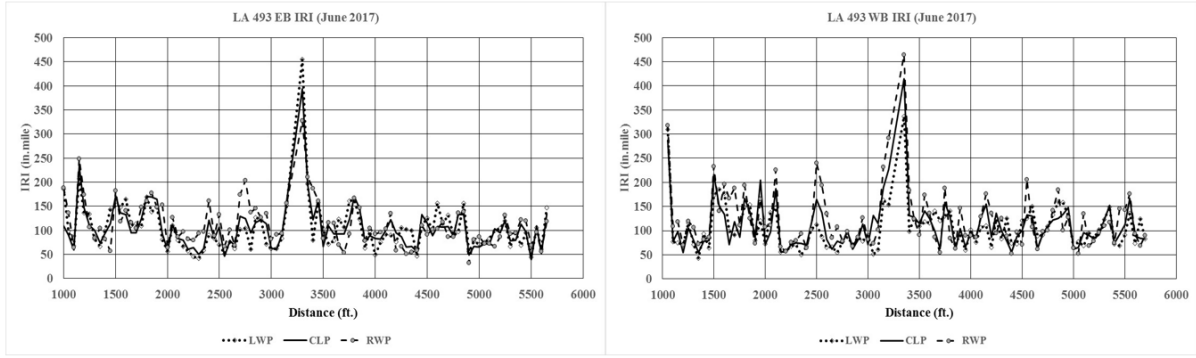


**Figure 26**  
**EB and WB IRI values for the June 2017 assessment**

**Table 20**  
**IRI statistical results for the June 2018 assessment**

Variable (2018)	N	Mean (in./mile)	Fisher Pairwise Grouping																		
1A_RWP_WB	4	207.07	A																		
1A_LWP_WB	4	188.28	A	B																	
1A_RWP_EB	4	180.01	A	B	C																
1A_CLP_WB	4	177.72	A	B	C	D															
4_RWP_WB	16	144.09	A	B	C	D	E														
1A_LWP_EB	4	138.77	A	B	C	D	E	F	G	H	I	J	K								
1_RWP_WB	12	138.36	A	B	C	D	E	F													
1A_CLP_EB	4	136.3	A	B	C	D	E	F	G	H	I	J	K								
4_RWP_EB	16	135.02		B	C	D	E	F													
1_LWP_EB	12	133.78		B	C	D	E	F	G	H	I	J	K								
4_CLP_EB	16	133.68		B	C	D	E	F													
4_CLP_WB	16	132.45		B	C	D	E	F					I								
3_RWP_WB	14	132.22		B	C	D	E	F					I								
1_RWP_EB	12	129.08		B	C	D	E	F	G	H	I	J	K								
4_LWP_EB	16	128.86		B	C	D	E	F	G	H	I	J	K								
1_CLP_EB	12	125.46		B	C	D	E	F	G	H	I	J	K								
1_LWP_WB	12	123.43		B	C	D	E	F	G	H	I	J	K								
4_LWP_WB	16	122.33		B	C	D	E	F	G	H	I	J	K								
1_CLP_WB	12	121.33		B	C	D	E	F	G	H	I	J	K								
3_RWP_EB	14	117.65			C	D	E	F	G	H	I	J	K								
2_RWP_WB	14	117.64			C	D	E	F	G	H	I	J	K								
5_RWP_WB	16	117.59			C	D	E	F	G	H	I	J	K								
2_RWP_EB	14	116.96			C	D	E	F	G	H	I	J	K								
5_LWP_WB	16	110.63				D	E	F	G	H	I	J	K								
3_CLP_WB	14	110.01				D	E	F	G	H	I	J	K								
2_CLP_WB	14	109.69				D	E	F	G	H	I	J	K								
5_CLP_WB	16	108.35					E	F	G	H	I	J	K								
5_CLP_EB	16	108.29					E	F	G	H	I	J	K								
5_RWP_EB	16	107.2					E	F	G	H	I	J	K								
5_LWP_EB	16	107					E	F	G	H	I	J	K								
6_RWP_WB	16	106.99					E	F	G	H	I	J	K								
2_CLP_EB	14	104.86					E	F	G	H	I	J	K								
6_RWP_EB	16	104.53					E	F	G	H	I	J	K								
6_CLP_WB	16	102.41					E	F	G	H	I	J	K								
2_LWP_WB	14	101.01					E	F	G	H	I	J	K								
6_LWP_WB	16	99.66						F	G	H	I	J	K								
3_CLP_EB	14	96.87						F	G	H	I	J	K								
2_LWP_EB	14	96.41						F	G	H	I	J	K								
3_LWP_EB	14	92.83						F	G	H	I	J	K								
3_LWP_WB	14	88.63										I	J	K							
6_CLP_EB	16	87.31										H									K
6_LWP_EB	16	87.15								G	H			J	K						

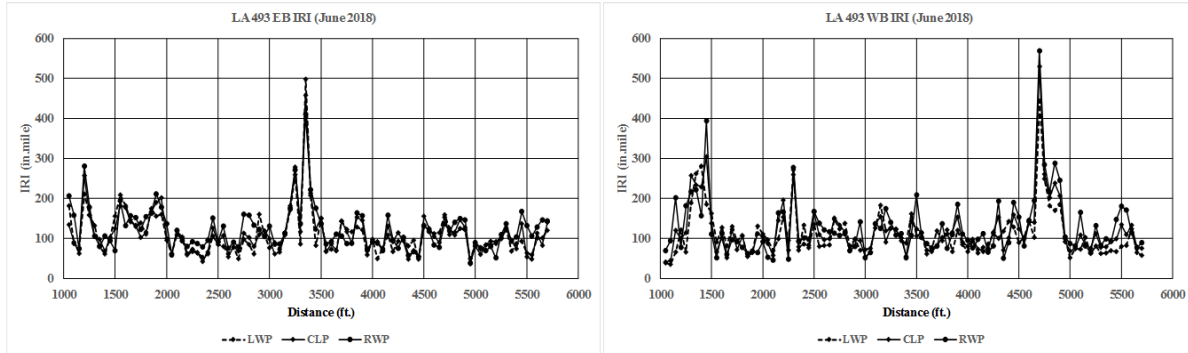


**Figure 27**  
**EB and WB IRI values for the June 2018 assessment**

**Rutting**

Tables 21 and 22 present the results from the statistical analysis for rutting. The variables were rutting values from the LWP and RWP for each site in both the EB and WB directions for the June 2017 and June 2018 assessments. There were 28 variables per assessment for the rutting data acquired on this project. Regarding the June 2017 and 2018 assessments, the mean values were represented by 13 distinct pairwise groups, indicating a high degree of variability in rutting amongst the groups.

Table 23 presents the statistical analysis for rutting modeled as overall groups. In this case, rutting values were averaged for the LWP and RWP for all the sites in both directions and both assessments (June 2017 and June 2018). For example, the June 2017 rutting values from the LWP from each of the six sites for the EB lane were grouped together as one group and labeled EB\_LWP\_2017. With this method, it could be determined if there were any overall differences between wheel paths, directions, and assessment years for the project. There were eight variables for this data set. The results indicated that the mean values were represented by 4 groups implying that there was high variability in the data set.

**Table 21**  
**Rutting statistical results for the June 2017 assessment**

Variable (2017)	N	Mean (in.)	Fisher pairwise grouping														
1_RWP_EB_17	12	0.0985	A														
3_RWP_EB_17	14	0.08107	A														
3_RWP_WB_17	14	0.04979	B														
4_LWP_WB_17	16	0.04231	B	C													
3_LWP_WB_17	14	0.04114	B	C													
5_RWP_WB_17	16	0.04056	B	C													
1_RWP_WB_17	12	0.03867	B	C													
1A_LWP_WB_17	4	0.038	B	C	D	E	F	G	H								
1_LWP_WB_17	12	0.03683	B	C													
4_RWP_EB_17	16	0.0355	B	C													
2_RWP_EB_17	14	0.03393	B	C			F										
6_LWP_WB_17	16	0.03331	B	C			F										
6_RWP_WB_17	16	0.03		C	D	F	G										
5_RWP_EB_17	16	0.02888		C	D	E	F	G	H								
2_RWP_WB_17	14	0.02864		C	D	E	F	G	H								
4_RWP_WB_17	16	0.02513		C	D	E	F	G	H								
1A_RWP_EB_17	4	0.025	B	C	D	E	F	G	H	I	J	K	L	M			
6_RWP_EB_17	16	0.02463		C	D	E	F	G	H								
2_LWP_WB_17	14	0.0235		C	D	E	F	G	H								
1A_RWP_WB_17	4	0.02125	B	C	D	E	F	G	H	I	J	K	L	M			
5_LWP_WB_17	16	0.01581					F	G	H	I	J	K	L	M			
6_LWP_EB_17	16	0.01044				E			H	I	J	K	L	M			
5_LWP_EB_17	16	0.00263															M
2_LWP_EB_17	14	0.00193														L	M
3_LWP_EB_17	14	0.00079											K	L	M		
1A_LWP_EB_17	4	0.0005			D	E		G	H	I	J	K	L	M			
4_LWP_EB_17	16	0.00031									J	K	L	M			
1_LWP_EB_17	12	0									I	J	K	L	M		

**Table 22**  
**Rotting statistical results for the June 2018 assessment**

Variable	N	Mean (in.)	Fisher pairwise grouping																				
3_RWP_EB_18	14	0.08729	A																				
1_RWP_EB_18	12	0.07025	A	B																			
3_RWP_WB_18	14	0.06321		B																			
3_LWP_WB_18	14	0.05586		B	C																		
6_LWP_WB_18	16	0.03794			C	D																	
4_LWP_WB_18	16	0.03713			C	D	E																
2_LWP_WB_18	14	0.03293				D	E	F															
1_LWP_WB_18	12	0.03292				D	E	F															
1A_LWP_WB_18	4	0.02475			C	D	E	F	G	H	I	J	K	L	M								
1A_RWP_EB_18	4	0.022				D	E	F	G	H	I	J	K	L	M								
4_RWP_WB_18	16	0.02175				D	E	F	G														
4_RWP_EB_18	16	0.02094				D	E	F	G	H				K									
6_LWP_EB_18	16	0.01837				D	E	F	G	H	I	J	K	L	M								
5_LWP_WB_18	16	0.01744					E	F	G	H	I	J	K	L	M								
2_RWP_EB_18	14	0.01286						F	G	H	I	J	K	L	M								
5_RWP_EB_18	16	0.01244						F	G	H	I	J	K	L	M								
5_RWP_WB_18	16	0.01031							G	H	I	J	K	L	M								
6_RWP_EB_18	16	0.00838							G	H	I	J	K	L	M								
1A_RWP_WB_18	4	0.004						F	G	H	I	J	K	L	M								
4_LWP_EB_18	16	0.003							G	H	I	J	K	L	M								
3_LWP_EB_18	14	0.00186							G	H	I	J	K	L	M								
2_RWP_WB_18	14	0.00179							G	H	I	J	K	L	M								
1_RWP_WB_18	12	0.00167							G	H	I	J	K	L	M								
6_RWP_WB_18	16	0.00156													K	L	M						
1A_LWP_EB_18	4	0.00025							G	H	I	J	K	L	M								
5_LWP_EB_18	16	0.00013												J			M						
2_LWP_EB_18	14	0												I	J		L	M					
1_LWP_EB_18	12	0												H	I	J	K	L	M				

**Table 23**  
**Overall rutting statistical results**

Variable	N	Mean (in.)	Fisher pairwise grouping			
EB_RWP_2017	92	0.04691	A			
WB_LWP_2018	92	0.03497		B		
WB_RWP_2017	92	0.03454		B		
EB_RWP_2018	92	0.03262		B		
WB_LWP_2017	92	0.0322		B		
WB_RWP_2018	92	0.01613			C	
EB_LWP_2018	92	0.00403				D
EB_LWP_2017	92	0.00276				D

Previous discussions for the statistical analysis were based on mean values for the segments in each test site (Tables 21 and 22) or for the overall grouping of the sites (Table 23). The following section discusses the maximum rutting values measured in each test site.

### **Maximum Rutting EB**

Figures 28 and 29 present the rutting measurements for Sites 1 to 6 on the assessment dates of June 2017 and June 2018. DOTD considers rutting values greater than 0.5 in. to be significant and in need of mitigation. It is probable that the significant rutting at some locations were due to weakening of the pavement structure due to volumetric changes in the embankment as well as depressions caused by movements in the embankment. For Site 1, the maximum rutting in June 2017 in the RWP was 0.386 in. and 0.74 in. a year later in June 2018 indicating that rutting in those locations are increasing. Site 2 showed a similar pattern with the maximum rutting in the RWP being 0.713 in. in June 2017 and 0.205 in. on June 2018. The reason for the decrease in the maximum rutting between June 2017 and June 2018 is unknown. The maximum rutting values for Site 3 in the RWP were 0.382 in. on June 2017 and 0.232 in. on June 2018. Site 4 had maximum rutting values in the RWP of 0.953 in. on June 2017 and 0.28 in. on June 2018. As with Site 2, the authors are uncertain of the decrease in maximum rutting between June 2017 and June 2018. The maximum rutting values in the RWP for Site 5 were 0.673 in. and 1.2 in. on June 2017 and June 2018, respectively. Site 6 had maximum rutting values in the RWP of 0.953 in. and 1.685 in. on June 2017 and June 2018, respectively. Site 6 had the highest maximum rut depth in the EB direction.

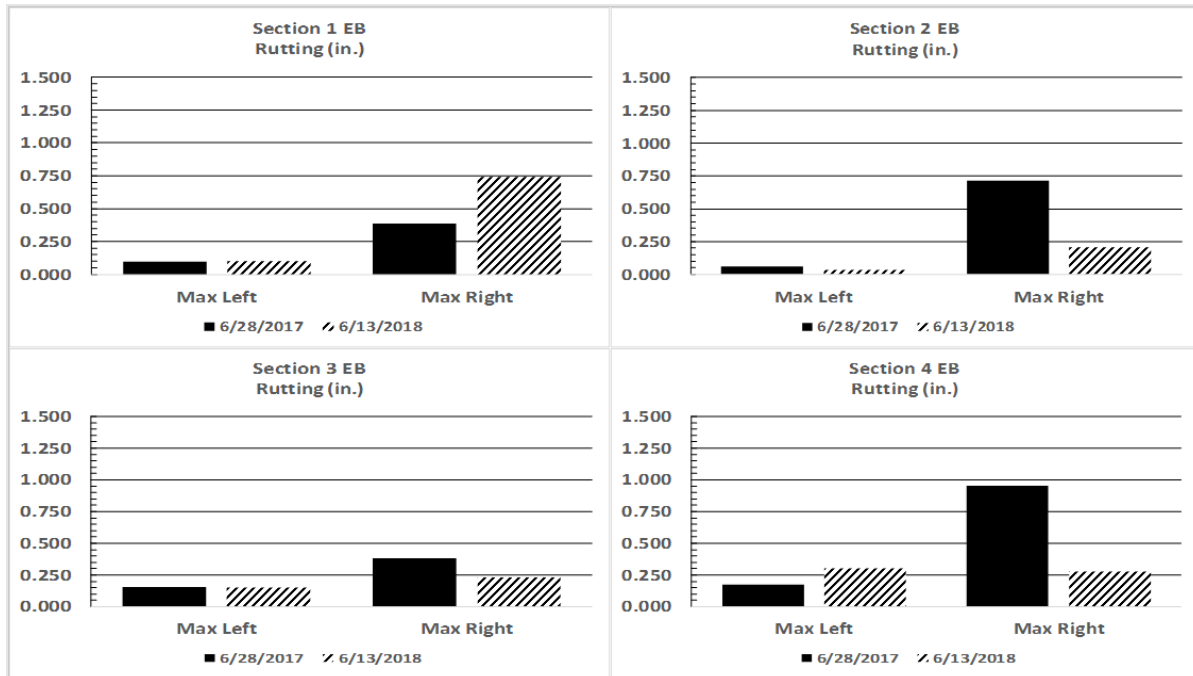


**Figure 28**  
EB maximum rutting for Sites 1 to 4

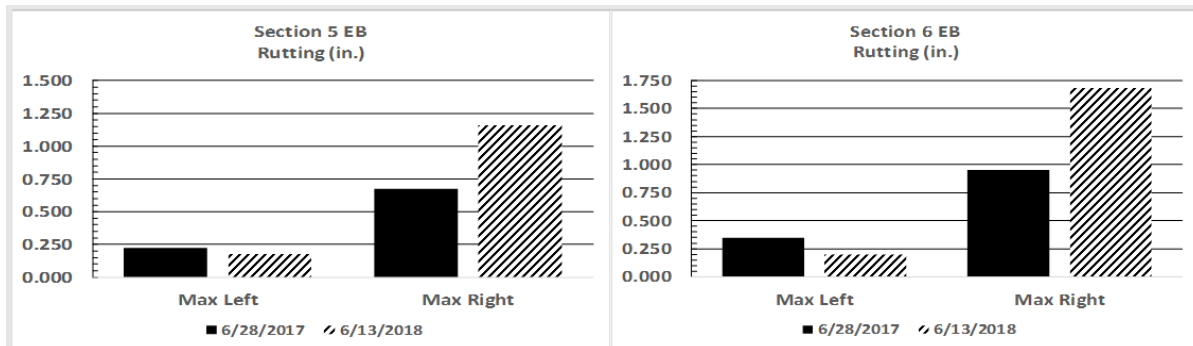


**Figure 29**  
EB maximum rutting for Sites 5 and 6

### Maximum Rutting WB

Figures 30 and 31 present the rutting measurements for Sites 1 to 6 on the assessment dates of June 2017 and June 2018. On Site 1, the maximum rutting depth in the RWP was 0.276 in. and 0.858 in. on June 2017 and June 2018 respectively. Site 2 had maximum rutting depths in the RWP of 0.807 in. for June 2017 and 0.122 in. for June 2018. The reason for the decrease in the rutting depths between June 2017 and June 2018 is unknown but may be due to volumetric changes in the embankment. The maximum rutting depth in the RWP for Site 3 was 0.268 in. and 0.850 in. on June 2017 and June 2018. respectively. Site 4 had maximum

rutting depths on the RWP of 1.236 in. and 0.929 in. in June 2017 and June 2018, respectively. Regarding Site 5, the maximum rutting depth in the RWP in June 2017 was 0.824 in. and in June 2018 it was 0.965 in. On Site 6, the maximum rutting depth on the RWP was 1.118 in. in June 2017 and 0.118 in. in June 2018.

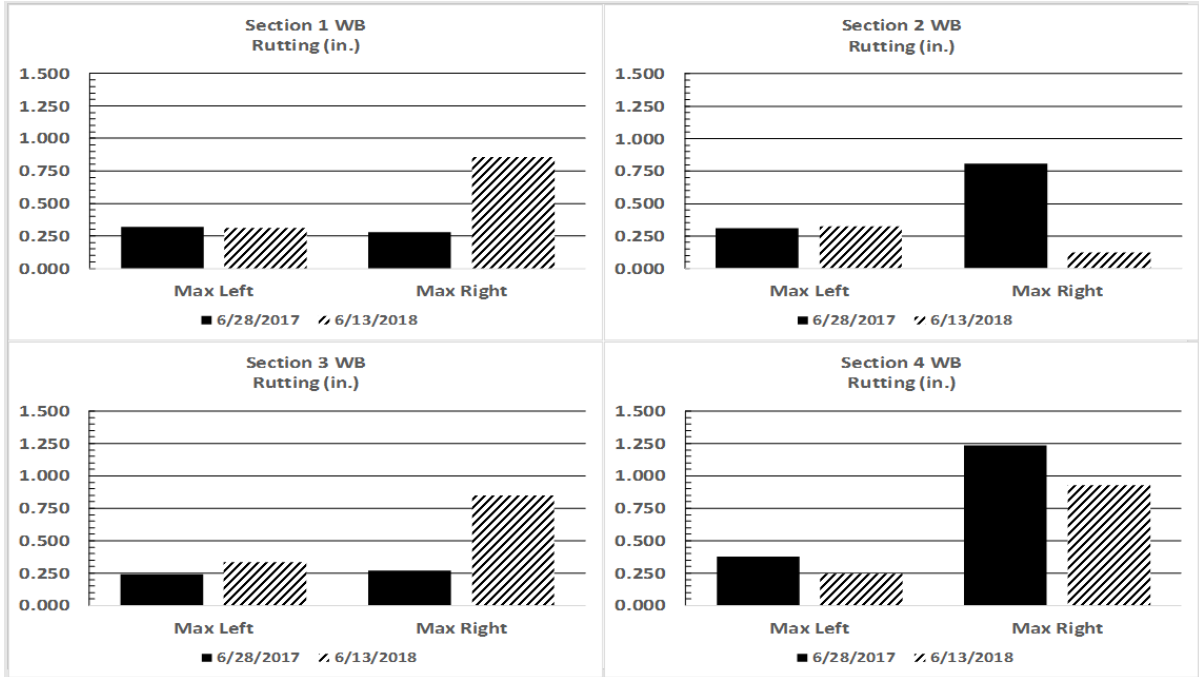


**Figure 30**  
WB maximum rutting for Sites 1 to 4

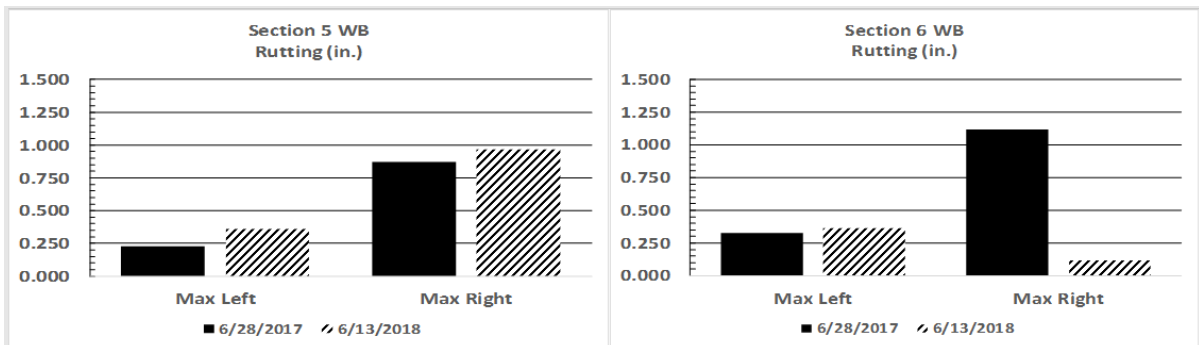


**Figure 31**  
WB maximum rutting for Sites 5 and 6

### Longitudinal Cracking

Table 24 and Table 25 presents the results from the statistical analysis for the June 2017 and June 2018 assessments, respectively. Figure 32 presents graphically the data that was used in these analyses. Longitudinal cracking is abbreviated as (LNCR) in Tables 24 and 25.

Regarding the June 2017 assessment, there were 14 variables as presented in Table 24. The results indicated that they could be placed into 8 different groups which implies that there was high degree of variability amongst the sites [54-55].

There were 14 variables for June 2018 assessment for the longitudinal cracking data acquired on this project [54-55]. The results from the June 2018 assessment groups implied that the data could be placed into 5 different groups implying less variability amongst the groups than the June 2017 group. As with the IRI and rutting data, high variability was present in the longitudinal cracking data.

Table 26 presents the statistical analysis for longitudinal cracks modeled as overall groups. In this case, longitudinal crack values were averaged for all the sites in both directions and both assessments (June 2017 and June 2018). For example, the June 2017 longitudinal crack values from the each of the six sites for the EB lane were grouped together as one group and labeled LNCR\_EB\_2017. The mean values presented in Table 26 represent the average of all sites (1-6) for that variable. Through this method, it could be determined if there were any overall differences between directions and assessment years for the project. There were 4 variables for this data set. The results indicated that the mean values were represented by 2 groups. There was no significant difference in the EB direction between the June 2017 and June 2018 assessment and the same was true for the WB direction. However, there was a significant difference between the EB and WB direction with the EB direction having higher means.

**Table 24**  
**Longitudinal cracking statistical analysis for June 2017**

Variable	N	Mean (ft.)	Fisher pairwise groupings							
5_LNCR_EB_17	16	62.71	A							
5_LNCR_WB_17	16	51.71	A	B						
6_LNCR_EB_17	16	46.19		B	C					
4_LNCR_EB_17	16	34.09			C	D				
3_LNCR_EB_17	14	32.3			C	D	E			
6_LNCR_WB_17	16	26.6				D	E	F		
2_LNCR_EB_17	14	21.64				D	E	F	G	
3_LNCR_WB_17	14	21.16				D	E	F	G	
2_LNCR_WB_17	14	15.05					E	F	G	H
1_INCR_EB_17	12	12.86						F	G	H
1_INCR_WB_17	12	5.89							G	H
1A_LNCR_EB_17	4	5.35						F	G	H
4_LNCR_WB_17	16	3.97								H
1A_LNCR_WB_17	4	0.8							G	H

**Table 25**  
**Longitudinal cracking statistical analysis for June 2018**

Variable	N	Mean (ft.)	Fisher pairwise groups							
5_LNCR_EB_18	16	63.56	A							
5_LNCR_WB_18	16	61.99	A							
6_LNCR_EB_18	16	47.12	A	B						
4_LNCR_EB_18	16	44.83		B						
3_LNCR_EB_18	14	34.61		B	C					
6_LNCR_WB_18	16	28.04				C	D			
3_LNCR_WB_18	14	23.31				C	D	E		
2_LNCR_WB_18	14	22.66				C	D	E		
2_LNCR_EB_18	14	19.49				C	D	E		
1_INCR_EB_18	12	14.16					D	E		
1_INCR_WB_18	12	9.15							E	
4_LNCR_WB_18	16	6.22								E
1A_LNCR_EB_18	4	4.66						D	E	
1A_LNCR_WB_18	4	3.95						D	E	

**Table 26**  
**Overall statistical grouping for longitudinal cracks**

Variable	N	Mean (ft.)	Grouping	
LNCR_EB_2018	92	36.53	A	
LNCR_EB_2017	92	34.24	A	
LNCR_WB_2018	92	24.82		B
LNCR_WB_2017	92	20.18		B

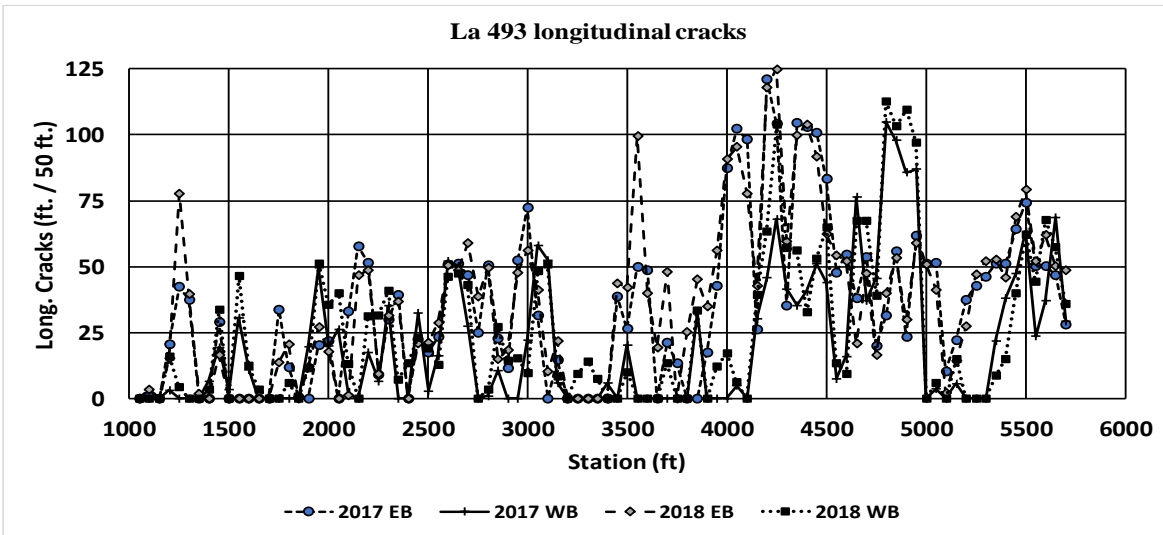


**Figure 32**

Longitudinal cracks for the EB and WB directions for the June 2017 and June 2018 assessments

### Falling Weight Deflectometer

#### Structural Number

Table 27 presents the  $SN_{eff}$  statistical results and equivalent thickness analyses calculated from FWD readings in July 2018. Regarding the  $SN_{eff}$  thickness results, there were 14 variables used in the Fisher pairwise comparisons. The results indicated that there were 3 possible pairwise groups for the dataset. Unlike the IRI, rutting, and longitudinal cracking data, there was less variability amongst the test sites. It should be noted that only test Site 1A had  $SN_{eff}$  values that exceeded the  $SN_{new}$ . This also is the site where no trees were present and had a 2 ft. thick sand interlayer. In the east bound direction for Site 1, the  $SN_{eff}$  was equivalent to  $SN_{new}$  and also had a sand interlayer but had trees present. So in general, the sites with sand interlayers retained their newly constructed strength. All other sections had  $SN_{eff}$  values less than  $SN_{new}$ .

Referring to the equivalent thicknesses presented in Table 27, positive values indicate that the section is stronger than its anticipated value when newly constructed while negative values indicate the amount of AC thickness (in.) that would be required to restore it to its newly constructed condition. Sites 1A (EB and WB) and Site 1 EB were the only sites with AC equivalent thickness values above zero. Those values ranged from 0 to 0.57 in. The remainder of the sites had values less than zero implying that they were structurally deficient. Their equivalent AC values ranged from -0.20 to -2.61 in. Sites 4 EB and 5 WB were the most distressed sites with structural deficiencies of 2.40 and 2.61 in of equivalent AC, respectively. The measured structurally deficient values due to inundation fall within the range discovered by others [8-10].

**Table 27**  
**SN<sub>eff</sub> and damage statistical results for the June 2018 assessment**

Variable (2018)	Statistical analysis					AC equivalent thickness analysis			Rank (Strongest to weakest)
	N	Avg. (SN <sub>eff</sub> )	Fischer pairwise groups			SN <sub>new</sub>	SN <sub>eff</sub> - SN <sub>new</sub>	AC equivalent (in.)	
1A_EB_2018	3	2.85	A			2.6	0.25	0.57	1
1A_WB_2018	3	2.70	A	B		2.6	0.10	0.22	2
1_EB_2018	3	2.62	A	B		2.6	0.02	0.05	3
2_WB_2018	3	2.55	A	B		3.1	-0.55	-1.24	11
3_EB_2018	3	2.51	A	B		2.6	-0.09	-0.20	4
1_WB_2018	3	2.40	A	B		2.6	-0.20	-0.45	5
2_EB_2018	3	2.40	A	B		3.1	-0.70	-1.59	12
3_WB_2018	3	2.40	A	B		2.6	-0.20	-0.46	6
6_WB_2018	3	2.33	A	B		2.6	-0.27	-0.62	7
6_EB_2018	3	2.32	A	B		2.6	-0.28	-0.63	8
4_WB_2018	3	2.29	A	B		2.6	-0.31	-0.70	9
5_EB_2018	3	2.19		B		2.6	-0.41	-0.93	10
4_EB_2018	3	1.54			C	2.6	-1.06	-2.40	13
5_WB_2018	3	1.45			C	2.6	-1.15	-2.61	14

### Subgrade Resilient Modulus

There were 14 variables used in the subgrade M<sub>r</sub> statistical analysis as presented in Table 28. The data were represented by 4 pairwise groups and the mean values ranged from 5.1 to 3.9 ksi. The measured subgrade M<sub>r</sub> values are consistent with weak saturated clay subgrades in Louisiana. Unlike the IRI, rutting, and longitudinal cracking data, there was less variability amongst the test sites.

**Table 28**  
**Subgrade M<sub>r</sub> statistical results**

<b>Variable</b>	<b>N</b>	<b>Mean (ksi)</b>	<b>Fisher pairwise groups</b>			
1A_Sub_EB_18	3	5.1	A			
1A_Sub_WB_18	3	5.1	A			
2_Sub_EB_18	3	4.9	A	B		
6_Sub_WB_18	3	4.8	A	B	C	
3_Sub_WB_18	3	4.6	A	B	C	D
1_Sub_WB_18	3	4.5	A	B	C	D
1_Sub_EB_18	3	4.4	A	B	C	D
2_Sub_WB_18	3	4.3		B	C	D
4_Sub_WB_18	3	4.3		B	C	D
5_Sub_WB_18	3	4.3		B	C	D
4_Sub_EB_18	3	4.2			C	D
6_Sub_EB_18	3	4.1			C	D
5_Sub_EB_18	3	4.0				D
3_Sub_EB_18	3	3.9				D

## CONCLUSIONS

Strong evidence of damage caused by inundation was provided by the testing conducted in this research project. The evidence supporting this claim was based on three major sources:

1. A rod and level cross-section survey taken approximately one month prior to the first inundation event and subsequent cross-section surveys taken after the three inundation events.
2. Pavement assessments with LTRC's profiling and imaging vehicle in June 2017 and June 2018.
3. Pavement assessment with the FWD in July 2018. Data from the FWD were  $SN_{eff}$  and subgrade  $M_r$ .

Differential movements of the roadway surface caused by inundation were clearly demonstrated from the cross-section surveys conducted from December 2015 to March 2018. The first cross-section survey was conducted in December 2015, approximately one month after the newly constructed roadway was open to traffic. Shortly thereafter, the roadway was inundated from approximately January 2016 to March 2016. As soon as the waters receded, another cross-section survey was conducted in April 2016. The cross-section survey clearly demonstrated the elevation increases caused by the inundation. In April of 2016, the increases in elevation at the roadway centerline ranged from 2.44 mm to 44.50 mm. With the exception of cross-section Site 1A, cross-section points right and left of the centerline increased with no adjacent point having the same magnitude of increase within each cross-section. This trend continued in subsequent cross-section surveys. In March 2018, the elevation increases at the centerline of the roadway ranged from 0.26 mm to 59.51 mm. The highest measured increase in elevation throughout the survey period (December 2015 to March 2018) was 63.47 mm. Such increases, especially since they varied from location to location in the cross-section will significantly damage the entire roadway section (pavement, base course, and embankment). Cross-section 1A is unique amongst the sites in that it was the only location where trees were not present adjacent to the right-of-way. When compared to the other cross-section sites, it is clearly evident the effect that trees have on the subgrade in that much more significant elevation changes occurred in those sites after the inundation events. Movements of differing proportions throughout the service life of the pavement will adversely affect its performance and reduce its service life.

High variability in the IRI measurements also provided evidence of damage caused by the three inundation events. There was such a significant variation in the June 2017 assessment data that statistical pairwise comparisons could not be calculated. Statistical analyses of the

IRI data from the June 2018 yielded 11 distinct groups, implying that a high variation existed in the data. Results for the IRI data implied that (1) there were high degrees of differential profile changes in the roadway surface, (2) the IRI was significantly higher than it should have been for a roadway of its service age, and (3) there was a high degree of IRI variation amongst the sites.

As with the IRI data, there were high degrees of variability in the rutting data. The statistical analysis implied that the data could be placed in 13 distinct groups for both the June 2017 and June 2018 data. The rutting data was also modeled as overall groups. In this case, rutting values were averaged for the LWP and RWP for all the sites in both directions (EB and WB) and both assessment years (June 2017 and June 2018). The results indicated that this data could be placed in 4 distinct groups implying that high variability existed. The maximum rut depth measured was 1.685 in. on Site 6 in the EB direction.

As with the IRI, the statistical analyses for the longitudinal crack data implied that there were high degrees of variability amongst the test sites. Data from the June 2017 assessment could be placed into 8 distinct groups while data from the June 2018 group could be placed in 5 distinct groups. The longitudinal crack data were also compared as overall groups. In this case, longitudinal crack data were averaged for all sites based upon direction (EB and WB) and assessment year (June 2017 and June 2018). The results indicated that significant differences existed between the EB and WB directions.

From FWD data, the  $SN_{eff}$  and subgrade  $M_r$  were statistically analyzed. Regarding the  $SN_{eff}$ , there were 3 distinct groups indicating less variability than IRI, rutting, and longitudinal cracking data sets. When the  $SN_{eff}$  was compared to the  $SN_{new}$ , structural deficiencies ranging from 0.2 to 2.61 of equivalent AC were discovered. The measured structurally deficient values due to inundation are within the ranges discovered by others [8-10]. The statistical analysis of the subgrade  $M_r$  values implied that there were 4 distinct groups with mean values ranging from 3.9 to 5.1 ksi. The measured  $M_r$  values are consistent with weak saturated clay subgrades in Louisiana.

## **RECOMMENDATIONS**

Extreme weather events are becoming more frequent. There have been at least three major inundation events caused by either unnamed oceanic storms or hurricanes resulting in record flooding in the USA since 2016. Several studies, including this one have shown that inundation causes measurable structural damage to the pavements. It is recommended that DOTD identify flood prone roadways and conduct structural testing on them either annually or biennially so that before and after statistical testing of the pavement structure can be conducted. Having this type of program will aide in determining the amount of damage caused by future inundation events.



## ACRONYMS, ABBREVIATIONS, AND SYMBOLS

AASHTO	American Association of State Highway and Transportation
AC	Asphaltic concrete
CLP	center lane path
cm.	centimeter(s)
DOTD	Louisiana Department of Transportation and Development
EB	east bound
FEMA	Federal Emergency Management Agency
FHWA	Federal Highway Administration
ft.	foot (feet)
FWD	falling weight deflectometer
in.	inch(es)
IRI	International Roughness Index
LL	liquid limit
LNCR	longitudinal cracks
LTRC	Louisiana Transportation Research Center
LWP	left wheel path
m.	meter(s)
mm.	millimeter(s)
$M_r$	resilient modulus
N	number
NOAA	National Oceanic Atmospheric Association
RWP	right wheel path
$SN_{eff}$	in place structural number
$SN_{new}$	theoretical structural number of newly constructed pavement
WB	west bound



## REFERENCES

1. NOAA. “National Centers for Environmental Information (NCEI) U.S. Billion Dollar Weather and Climate Disasters.” (2018). <https://www.ncdc.noaa.gov/billions/>
2. Smith, A. and Matthews, J. “Quantifying Uncertainty and Variable Sensitivity within the U. S. Billion-dollar Weather and Climate Disaster Cost Estimates.” *Natural Hazards*. 2015. DOI:10.1007/s11069-015-1678-x
3. Federal Emergency Management Administration, Significant Flood Events, 2018, <https://www.fema.gov/significant-flood-events>. Accessed September 17, 2018.
4. Kopp, R. E., Horton R., Little, C. J., Mitrovica, M., Oppenheimer, D. J. Rasmussen, Strauss, B., and Tebaldi. C. “Probabilistic 21st and 22nd century sea-level projections at a global network of tide-gauge sites.” *Earth’s Future*, 2, pp. 383–406, 2014. DOI:10.1002/2014EF000239
5. Buchanan, M., Oppenheimer, M., and Koop, R. “Amplification of Flood Frequencies with Local Sea Level Rise and Emerging Flood Regimes.” IOP Publishing, *Environmental Research Letters*, 12 06-4009, 2017. <https://doi.org/10.1088/1748-9326aa6cb3>. Accessed September 17, 2018.
6. Gaspard, K., Zhang, Z., Gautreau, G., and Abufarsakh., M. “Assessment of Pavement Distresses Caused by Trees on Rural Highways.” Louisiana Transportation Research Center, Project Capsule 12-1P, 2012, [http://www.ltrc.lsu.edu/pdf/2012/capsule\\_12\\_1P.pdf](http://www.ltrc.lsu.edu/pdf/2012/capsule_12_1P.pdf).
7. Gaspard, K., and Zhang, Z. “Submerged Road Characteristics and Distresses on LA 493, Natchitoches Parish, State Project Number H.011071.” LTRC 18-04-TA-P, 2018.
8. Gaspard, K., Martinez, M., Zhang, Z., and Wu, Z. “Impact of Hurricane Katrina on Roadways in the New Orleans Area, Louisiana Transportation Research Center.” Technical Assistance Report No. 07-2TA, 2006.
9. Zhang, Z., Wu, Z., Martinez, M., and Gaspard, K. “Pavement Structures Damage Caused by Hurricane Katrina Flooding.” *Journal of Geotechnical and Geoenvironmental Engineering*,” 135(5), pp. 633-643, 2008.
10. Helali, K., Robson, M., Nicholson, R., and Bekheet, W. “Importance of a Pavement Management System in Assessing Pavement Damage from Natural Disasters: A Case Study to Assess the Damage from Hurricanes Katrina and Rita in Jefferson Parish, Louisiana.” In *Proceedings of the 7th International Conference on Managing Pavement Assets*, 10-21, 2008.
11. Vennapusa, P., White, D., and Miller, K. “Western Iowa Missouri River Flooding - Geo-Infrastructure Damage Assessment, Repair and Mitigation Strategies.” Center

- for Earthworks Engineering Research, Iowa State University, IHRB TR-638, 2013.
12. American Association of State Highway and Transportation Officials. "AASHTO Guide for Design of Pavement Structures." 1993.
  13. Sultana, M., Chai, G., Martin, Tim, and Chowdhury, S. "A Study on the Flood Affected Flexible Pavements in Australia." In *Proceedings of the 9th International Conference on Road and Airfield Pavement Technology*, 2015.
  14. Paterson, W. *Road Deterioration and Maintenance Effects: Models for Planning and Management*. HDM(III), 1987.
  15. Austroads. *Predicting Structural Deterioration of Pavements at a Network Level - Interim Models*. Sydney, NSW, Australia, 2010.
  16. Alam, M. and Zakaria, M. "Design and Construction of Roads in Flood Affected Areas." *Engineering Concern of Floods*, ISBN 984-823-002-5, 2002.
  17. Mallick, R., Tao, M., Daniel, J., Jacobs, J., and Veeraragavan. A. "Development of a Methodology and a Tool for the Assessment of Vulnerability of Roadways to Flood-Induced Damage." *Journal of Flood Risk Management* 10, pp. 301-313, 2017.
  18. Forrester, J. *World Dynamics*. Cambridge MA: Wright-Allen Press, 1971.
  19. Radzicki, J. "A Systems Dynamics Approach to Sustainable Cities." In *the Proceedings of the 13th International Systems Dynamics Conference*, 191-210, 1995.
  20. Sterman, J. "Sustaining Sustainability: Creating a Systems Science in a Fragmented Academy and Polarized World." In *M.P. Weinstein & R.E. Turner, eds. Sustainability Science: The Emerging Paradigm and the Urban Environment*. Springer, pp. 21-58, 2012.
  21. Green, W. and Ampt, G. "Studies of Soil Physics, Part I - The Flow of Air and Water Through Soils." *Journal of Agricultural Science*, 4, 1-24, 1911.
  22. Briaud, J. "Case Histories in Soil and Rock Erosion: Woodrow Wilson Bridge." In the 9th Ralph B. Peck lecture. *Journal of Geotechnical and Geoenvironmental Engineering*, 134, (10) pp.1425-1447, 2008.
  23. National Cooperative Highway Research Program. "Guide for Mechanistic-Empirical Design: Design Inputs." *Transportation Research Board*, 2004.
  24. Khan, M., Mesbah, M., Ferreira, L., and Williams, D. "Estimating Pavement's Flood Resilience." American Society of Civil Engineers, *Journal of Transportation Engineering*, Part B: Pavements, 2017.
  25. Khan, M. "Improvement of a Pavement Management System Incorporating Flooding." Ph.D. Thesis, School of Civil Engineering, University of Queensland, St. Lucia, Australia. 2017.
  26. Khan, M., Mesbah, M., Ferreira, L., and Williams, D. "Development a Road Deterioration Model Incorporation Flooding." In *the Proceedings of Transportation*

- Institute of Civil Engineering*, 167(5), pp. 322-333. 2014.
27. Khan, M., Mesbah, M., Ferreira, L., and Williams, D. "Development of Road Deterioration Models Incorporating Flooding for Optimum Maintenance and Rehabilitation Strategies." *Road Transportation Research Journal Australia-New Zealand Research Practices*, 23(1), pp. 3-24, 2014.
  28. Khan, M., Mesbah, M., Ferreira, L., and Williams, D. "Assessment of Flood Risks to Performance of Highway Pavements." In *Proceedings of Institute of Civil Engineers-Transport*, Thomas Telford, London. 2017.
  29. Sultana, M., Chai, G., Chowdhury, S., Martin, Tim, Anissimov, Y., and Rahman, A. "Rutting and Roughness of Flood-Affected Pavements: Literature Review and Deterioration Models." American Society of Civil Engineers, *Journal of Infrastructure Systems*, 24(2): 04018006, 2018.
  30. Sultana, M., Chai, G., Martin, Tim, and Chowdhury, D. "Modelling the Postflood Short Term Behavior of Flexible Pavements." *Journal of Transportation Engineering*, DOI: 10.1061/(ASCE)TE,1943-5436.0000873, 04016042. 2016.
  31. Sultana, M., Chai, G., Martin, T., and Chowdhury, S. "Modelling Rapid Deterioration of Flooded Pavements." *Road Transportation Research*, 25(2), 2016.
  32. Shamsabadi, S., Tari, Y., Birken, R., and Wang, M. "Deterioration Forecasting in Flexible Pavements Due to Floods and Snow Storms." In *the Proceedings of the 7th European Workshop on Structural Health Monitoring*, 2014.
  33. Jackson, N., and Puccinelli, J. "Effects of Multiple Freeze Cycles and Deep Frost Penetration." Long-Term Pavement Performance Data Analysis Support: National Pool fund Study TPF-5(013), 2006.
  34. Elshaler, M. "Assessing the Mechanical Response of Pavements During and After Flooding." Doctoral Dissertations 160. <https://scholars.unh.edu/dissertation/160>. 2017.
  35. National Cooperative Highway Research Program. "Laboratory Determination of Resilient Modulus for Flexible Pavement Design." *NCHRP Digest 285*, Transportation Research Board, 2004.
  36. Nelson, J., and Miller, D. *Expansive Soils, Problems and Practice in Foundation, and Pavement Engineering*. John E Wiley and Sons, 1992.
  37. American Society of Civil Engineers. "Expansive Clay Soils and Vegetative Influence on Shallow Foundations." *Geotechnical Special Publication Number 115*, 2001.
  38. Department of the Army USA. "Technical Manual TM 5-818-7, Foundations in Expansive Soils." September 1983.
  39. Terzaghi, K., Peck, R., and Mesri, G. *Soil Mechanics in Engineering Practice*. John

- Wiley and Sons, 1996.
40. Fredlund, D. and Rahardjo, H. *Soil Mechanics for Unsaturated Soil*. John Wiley and Sons, 1993.
  41. Lu, N. and Likos, W. *Unsaturated Soil Mechanics*. John Wiley and Sons, 2004.
  42. Wise, J. and Hudson, W. "An Examination of Expansive Clay Problems in Texas." Center for Highway Research, The University of Texas at Austin, Research Report Number 118-5, 1971.
  43. Sebasta, S. "Investigation of Maintenance Base Repairs Over Expansive Soils: Year 1 Report," Texas Transportation Institute, FHWA/TX-03/0-4395-1, 2002.
  44. Zornberg, J., Prozzi, J., Gupta, R., Luo, R., McCartney, J., Ferreira, J., and Nogueira, C. "Validating Mechanisms in Geosynthetic Reinforced Pavements." Center for Transportation Research, The University of Texas at Austin, 2008.
  45. Steinberg, M. *Geomembranes and The Control of Expansive Soils in Construction*. McGraw-Hill Professional, 1998.
  46. Al-Rawas, A. and Goosen, M. *Expansive Soils-Recent Advances in Characterization and Treatment*. Taylor and Francis, 2006.
  47. Biddle, P.G. *Tree Root Damage to Buildings, Volumes 1 and 2*. Willomead Publishing Ltd., 1998.
  48. Roberts, J., Jackson, N, and Smith, M. *Tree Roots in the Built Environment*. TSO Publications, 2006.
  49. Freeman, T., Driscoll, R., and Littlejohn, G. *Has Your House Got Cracks*. BRE and Thomas, The Elford Ltd, 2002.
  50. Croney, D., and Croney, P. *Design and Performance of Road Pavements*. Third Edition, Mcgraw Hill Professional, 2008.
  51. Louisiana Department of Transportation and Development, Standard Specifications for Roads and Bridges. 2016 Edition,  
[http://wwwsp.dotd.la.gov/Inside\\_LaDOTD/Divisions/Engineering/Standard Specifications/Pages/Standard%20Specifications.aspx](http://wwwsp.dotd.la.gov/Inside_LaDOTD/Divisions/Engineering/Standard Specifications/Pages/Standard%20Specifications.aspx)
  52. Little, D., Allen, D., and Bhasin, A. *Modeling and Design of Flexible Pavements and Materials*. Springer, 2017.
  53. Federal Highway Administration. "LTPP Manual for Falling Weight Deflectometer Measurements." Version 4.1, FHWA-HRT-06-132, 2006.
  54. Neter, J. Kutner, M., Nachtsheim, C. and Wasserman, W. *Applied Linear Statistical Models*. Irwin 3rd Edition, ISBN: 0-256-11736-5, 1996.
  55. Day, R., and Quinn, G. "Comparisons of Treatments after an Analysis of Variance in Ecology." *Ecological Monographs* 59: pp. 433-463. 1985.

56. Sultana, M., Chai, G., Martin, T., and Chowdhury, S. "Modeling the Postflood Short-term Behavior of Flexible Pavements." *ASCE Journal of Transportation Engineering*, 142(10). [https://doi.org/10.1061/\(asce\)te.1943-5436.0000873](https://doi.org/10.1061/(asce)te.1943-5436.0000873). 2016.
57. Wang, Y., Huang, Y., Rattanachot, W., Lau, K. K., and Suwansawas, S. "Improvement of Pavement Design and Management for More Frequent Flooding Caused by Climate Change." *Advances in Structural Engineering*, 18(4), pp. 487-496, 2015.
58. Witzak, M., Dragos, A., and Houston, W. "Guide for Mechanistic-Empirical Design of New and Rehabilitated Pavement Structures." Appendix DD-1: Resilient Modulus as a Function of Soil-Moisture-Summary of Predictive Models, Final Report 1-37A., 2000.
59. Yang, S., Huang, W., and Tai, Y. "Variation of Resilient Modulus with Soil Suction for Compacted Subgrade Soils." *Transportation Research Record: Journal of the Transportation Research Board*, 1913(1), pp. 99-106., 2005.
60. Krishna, A., Dey, A., and Sreedeeep, S. "Geotechnics for Natural and Engineering Sustainable Technologies." *GeoNEst Developments in Geotechnical Engineering*, Springer 1st Edition, DOI .org/10.1007/978-10-7221-0, 2018.









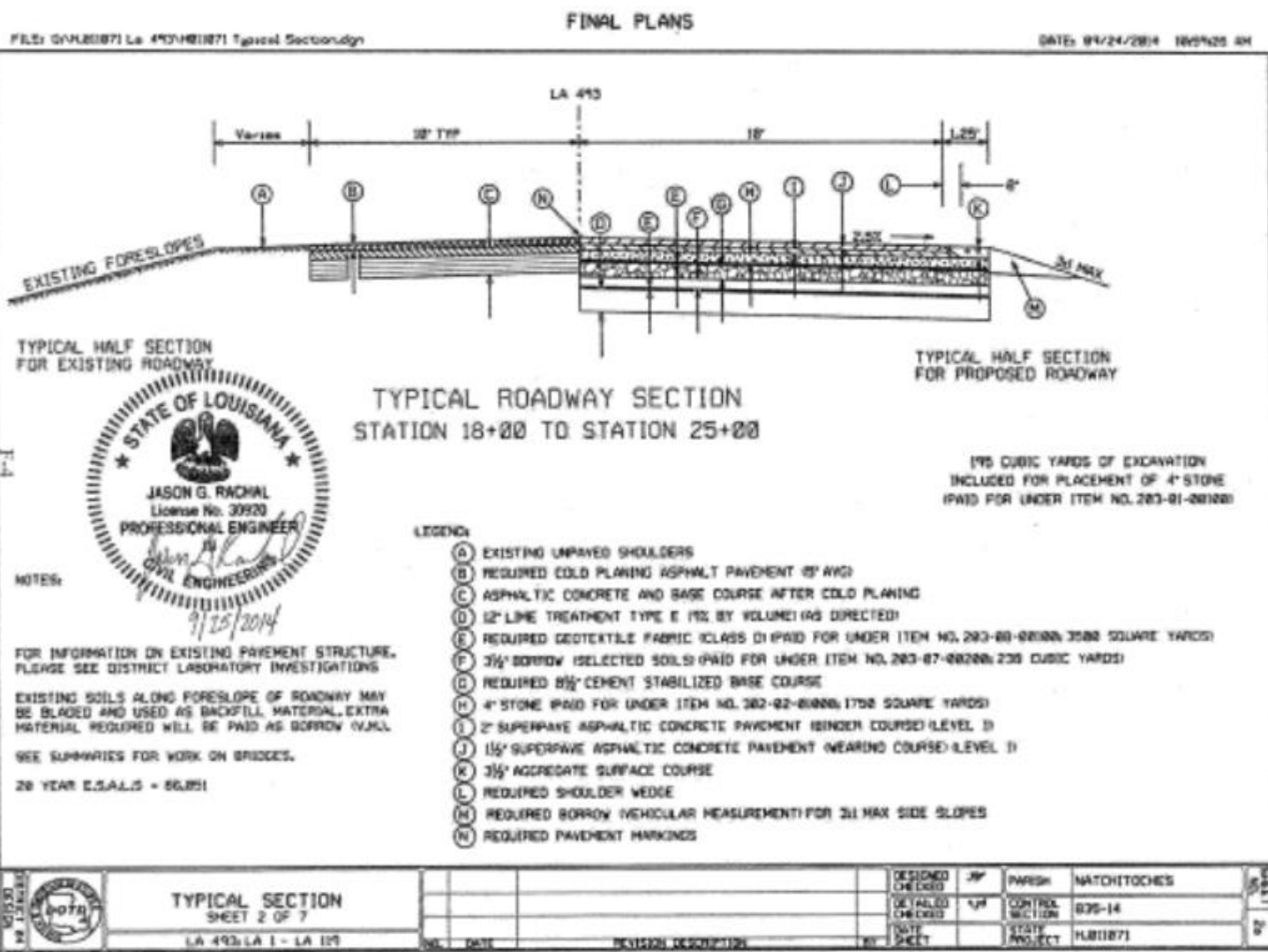


Figure 35  
Typical section for Site 2

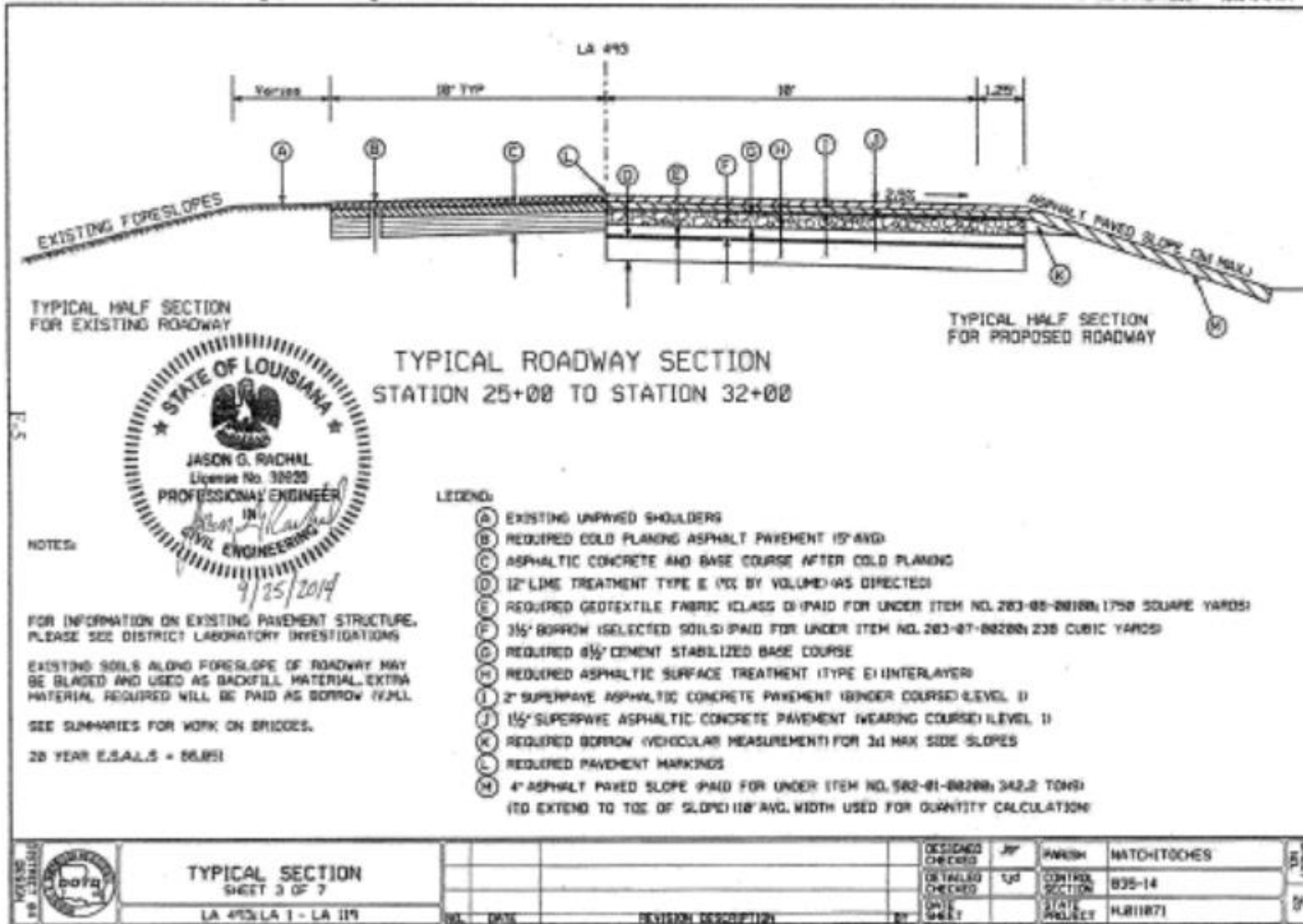


Figure 36  
Typical section for Site 3

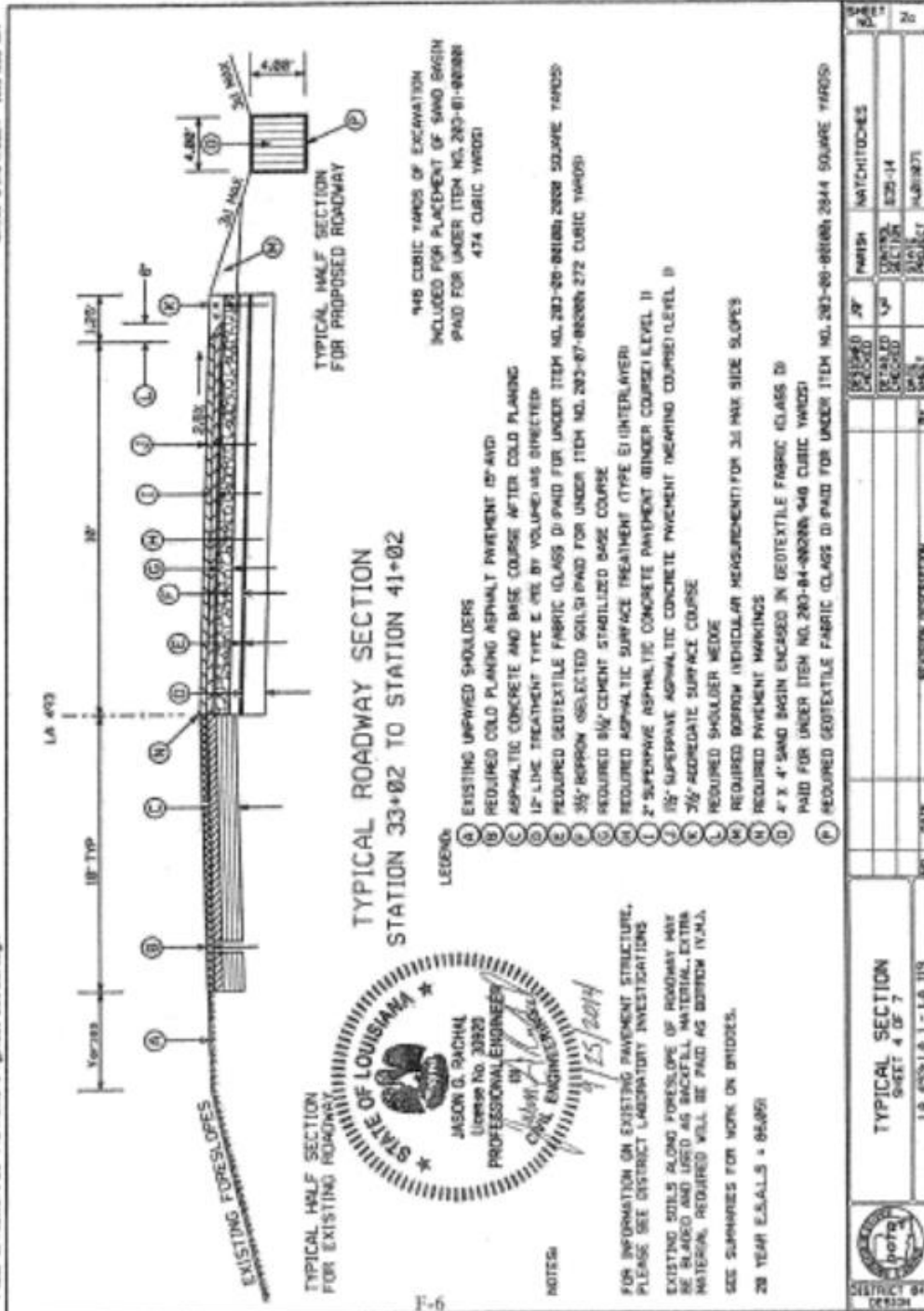


Figure 37  
 Typical section for Site 4

FINAL PLANS

FILE: D:\M\1187\LA 493\1187\Typical Section.dgn

DATE: 05/24/2014 11:00:24 AM

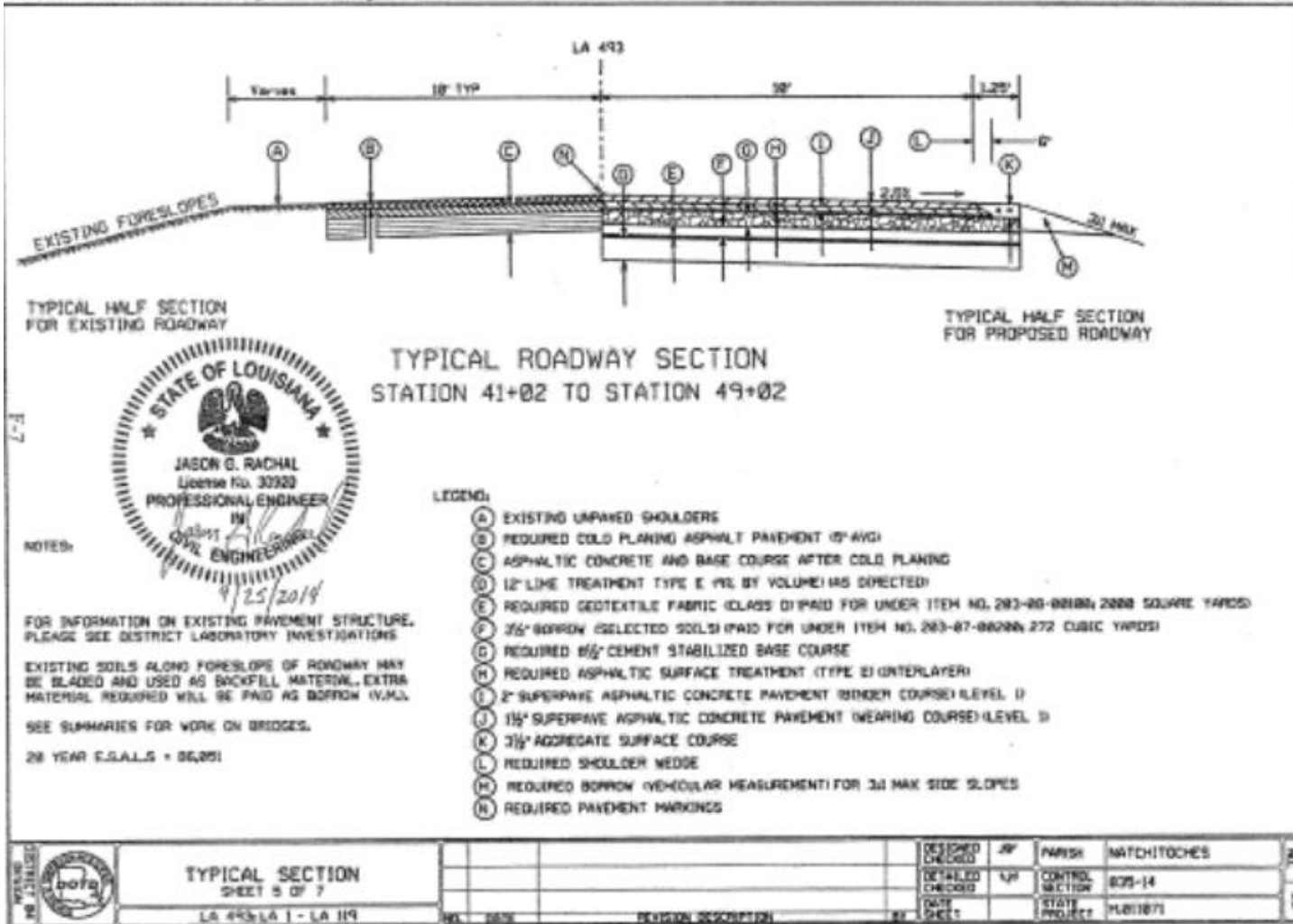


Figure 38  
Typical section for Site 5

FINAL PLANS

FILE# 490481871 LA 490481871 Typical Section.dgn

DATE: 05/24/2014 10:28:41 AM

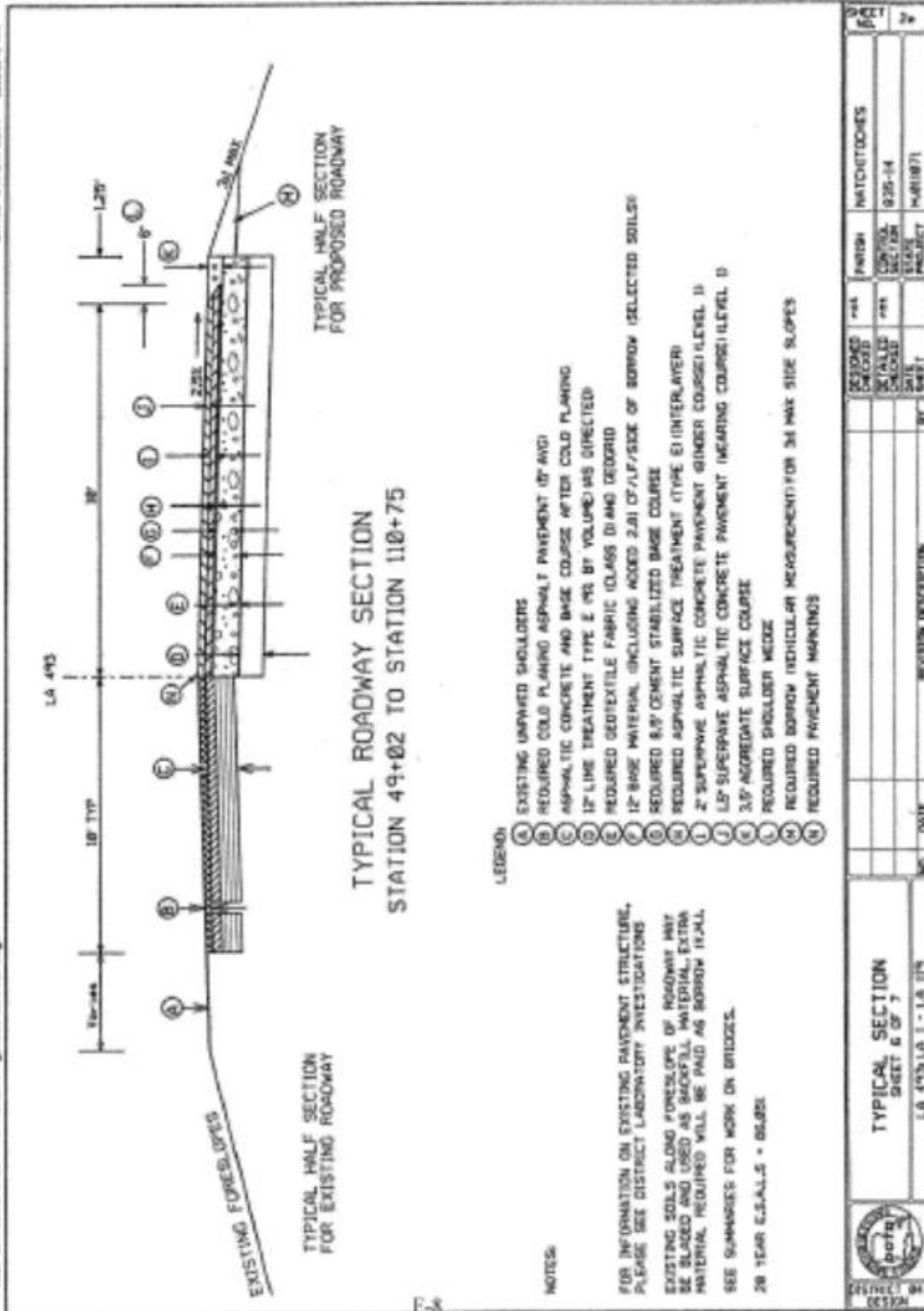


Figure 39  
Typical section for Site 6

This public document is published at a total cost of \$250. 42 copies of this public document were published in this first printing at a cost of \$250. The total cost of all printings of this document including reprints is \$250. This document was published by Louisiana Transportation Research Center to report and publish research findings as required in R.S. 48:105. This material was duplicated in accordance with standards for printing by state agencies established pursuant to R.S. 43:31. Printing of this material was purchased in accordance with the provisions of Title 43 of the Louisiana Revised Statutes.